Radar Observations of Near-Earth and Main-Belt Asteroids

Lance A. M. Benner
Jet Propulsion Laboratory, California Institute of Technology

Michael W. Busch
SETI Institute

Jon D. Giorgini
Jet Propulsion Laboratory, California Institute of Technology

Patrick A. Taylor
Arecibo Observatory

Jean-Luc Margot
University of California, Los Angeles

Abstract

Radar is a very powerful technique for characterizing near-Earth and main-belt asteroids and for improving their orbits. This results from radar's ability to spatially resolve objects that often cannot be resolved at comparable resolutions by other ground-based techniques. Radar has revealed binary and contact binary objects, at least two triple systems, non-principal axis rotators, objects whose radar reflectivity and circular polarization ratio have longitudinal variation, irregularly-shaped near-Earth asteroids, objects with metallic compositions, objects with rubble pile structures, and detailed radar images of main-belt asteroids that reveal complicated surfaces and substantial topographic relief. This chapter concentrates on the most significant advances in the field since publication of the radar chapter by Ostro et al. (2002) in *Asteroids III*. Detailed descriptions of asteroid radar observing techniques and terminology have appeared in Ostro (1993), Ostro et al. (2002; in *Asteroids III*), so we refer readers to those papers for background information. This chapter emphasizes the first ground-truth tests of asteroid shape models by spacecraft encounters, population trends among near-Earth and main-belt asteroids, results for selected objects, new observing techniques, improved capabilities at radar telescopes, and improvements in 3D shape modeling. We conclude with a discussion of future prospects.

Introduction

Planetary radar astronomy is an active form of observation in which the observer illuminates the target with radio waves having known properties and measures the reflected signal in order to investigate the physical properties of the target and to improve its orbit. Radar observations can occur during the day, in cloudy weather, during rain, and in a real sense represent a laboratory experiment on objects at distances of up to hundreds of millions of km.

The world's most sensitive facilities for radar observations of asteroids are the Arecibo Observatory and the Goldstone Solar System Radar. Arecibo has a diameter of 305 m and is the world's largest operational single-dish radio telescope. Arecibo's S-band system operates at a frequency of 2380 MHz (λ = 12.6 cm) and has a transmitter power of 900 kW. The dish is built into a sinkhole and cannot move; to point, the transmitters and receivers are suspended above the dish on azimuth and elevation rails that permit tracking of objects 360 deg in azimuth and within 20 deg of zenith. Arecibo is located in Puerto Rico at a latitude of +18 deg, so it is able to observe objects at declinations from -1 to +38 deg and see ~1/3 of the sky. Due to its pointing restrictions, Arecibo can track a given object for a maximum of 2.9 h/day. The highest range resolution currently available at Arecibo is 7.5 m/pixel.

The Goldstone Solar System Radar is located on the DSS-14 antenna at the National Aeronautics and Space Administration's (NASA) Goldstone Deep Space Communications Complex. DSS-14, hereafter referred to as "Goldstone," is part of the Deep Space Network. Goldstone has a diameter of 70 m, operates at a transmitter frequency of 8560 MHz (λ = 3.5 cm), and has a transmitter power of 450 kW. Goldstone is fully steerable and can track objects north of -35 deg, providing coverage for ~80% of the sky. The finest range resolution available at Goldstone is 3.75 m/pixel. Due to its higher transmitter frequency, Goldstone can provide 3.6x finer Doppler resolution than Arecibo in high signal-to-noise ratio (SNR) situations, which can be helpful for resolving small and/or slowly rotating objects.

The capabilities of Arecibo and Goldstone are complementary: Arecibo is about twenty times more sensitive and can detect objects to twice the distance, but Goldstone can track objects for several times longer, much farther north and south, and achieve higher resolutions in range and Doppler frequency. Arecibo is designed as an astronomical observatory and is easier to use and schedule on short notice. The primary mission at Goldstone is spacecraft communication and the facility is currently available for astronomical observations for <10% of the time. Target-of-opportunity observations are possible at Goldstone but more challenging to schedule than targets identified well in advance. For many of the best targets, both observatories are utilized to maximize the return on scientific investment. Due to the time it takes equipment to switch from transmitting to receiving, Arecibo can observe objects as close as 0.008 au and Goldstone can observe objects as close as 0.005 au. For closer objects, the 34 m DSS-13 antenna is often used to receive

echoes from Goldstone transmissions, although that bistatic configuration reduces the signal-to-noise ratios (SNRs) by a factor of ~6. The 100 m Green Bank Telescope is also available for bistatic observations using both Arecibo and Goldstone to transmit.

In practice, due to its greater sensitivity, Arecibo can detect significantly more near-Earth asteroids than is possible at Goldstone despite Arecibo's restricted pointing capabilities. The principal reason is that many near-Earth objects traverse Arecibo's declination window when they are still close enough for Arecibo to detect. The fraction of NEAs observable by Goldstone that are too far north or south for Arecibo to detect is ~5% (S. P. Naidu, pers. comm.).

Radar astrometry can produce dramatic improvements in asteroid orbits for recently discovered objects due to radar's high fractional precision of up to 1 part in 10^8. For example, for a single opposition object, including radar astrometry in the orbit solution typically increases the interval of Earth encounter statistical predictability by a factor of five from 80 to 400 years, on average, compared to a solution based only on optical measurements (Ostro and Giorgini 2004). The effects of radar astrometry on asteroid orbit determination have been discussed in several papers; for a detailed summary see Ostro and Giorgini (2004).

Recent Radar Detection History

The number of NEAs observed with radar has increased dramatically since publication of *Asteroids III*: from 120 at the end of 2002 to 508 at the end of 2014 (**Figure 1** and tabulated online at: http://echo.jpl.nasa.gov/asteroids/PDS.asteroid.radar.history.html). This is due largely to a six-fold increase in the number of near-Earth asteroid discoveries. During the decade after completion of the upgrade at Arecibo in the late 1990s, the average number of near-Earth asteroid radar detections was 20-30 annually. This jumped by a factor of ~3 in 2012 following increased NASA funding at Arecibo (and to a lesser extent at Goldstone) and due to greater access to telescope time for targets known well in advance. Many weak targets that had previously been ignored are now being observed. The minimum SNR threshold adopted for scheduling an asteroid for radar observations is typically ~30/day at Goldstone and ~15/day at Arecibo, although there are many instances where observations are attempted for weaker targets.

Obtaining time for target-of-opportunity observations at Goldstone has long been much more cumbersome than at Arecibo. At Arecibo submission of an urgent proposal can lead to scheduling observations within one day. At Goldstone it is necessary to coordinate radiation clearance with more than 25 government organizations whose airspace surrounds DSS-14; this process used to take up to several days, but recent improvements have shrunk this to < 2 days. It is also possible to observe objects on very short notice without radiation clearance by

reducing the transmitter power to 110 kW. Many targets-of-opportunity have been observed recently at both observatories by redirecting time previously scheduled for other asteroids. Radar delay-Doppler astrometry is used to update the orbit solution during the observations and is posted online shortly after the experiment is complete at: http://ssd.jpl.nasa.gov/?radar

Technological developments

Arecibo

One of the most significant developments at Arecibo has been an upgrade in the highest resolution available for delay-Doppler imaging. Shortly after the upgrade in 1999, the highest range resolution was 15 m/pixel by taking data with the Caltech Baseband Recorder (CBR), equipment originally designed for observing pulsars. However, the CBR was complicated to use, it did not permit real-time monitoring of the data (so the user did not know if there were echoes or problems until much later), and it didn't utilize the full bandwidth available from Arecibo's klystron amplifiers. In 2004, the "Portable Fast Sampler" (PFS) data-taking system designed and built by J. L. Margot became fully operational and provided range resolutions up to 7.5 m/pixel. The PFS is much more straightforward to use, can write data directly to disk rather than using striped tape drives, permits the user to check the data in near-real time, and has been upgraded, cloned, and installed at Goldstone and Green Bank. 7.5 m resolution is close to the theoretical limit of ~6 m imposed by the bandwidth of Arecibo's klystrons. A factor of two in range resolution yields pronounced differences in the detail visible in delay-Doppler radar images and nearly all of the strongest SNR targets observed at Arecibo now use 7.5 m resolution.

Goldstone

The most important improvement at Goldstone during the last decade has been the development of finer resolution delay-Doppler imaging using chirp waveforms. From 1992 to 2010, the finest range resolution at Goldstone was 18.75 m achieved by using binary phase coded waveforms. Although Goldstone's klystron amplifiers could be modulated at higher frequencies and in principle obtain higher resolutions, 18.75 m (with the frequency side lobes of binary phase-coded waveforms) is the finest resolution possible without violating Goldstone's frequency license. To achieve higher resolution without violating the license, linear frequency modulation (also known as chirping) was implemented (Slade et al. 2011). The chirp system improved the resolution at Goldstone by a factor of five from 18.75 m to 3.75 m, a resolution twice as fine as the highest resolution available at Arecibo. This illustrates another way in which the capabilities of Arecibo and Goldstone are complementary. The first asteroid observed with a range resolution of 3.75 m was 2010 AL30 (Slade et al. 2010), an object ~30 m in diameter that approached within 0.00086 au (0.3 lunar distances) in January 2010.

A five-fold improvement in resolution reveals considerably more detail than was previously possible and has yielded dramatic images of several objects a few hundred meters in diameter (or larger) such as (308635) 2005 YU55, (214869) 2007 PA8, (4179) Toutatis, 2014 HQ124, and (357439) 2004 BL86. For example, numerous impact craters and boulders are visible on the surface of 2005 YU55 (**Figure 2**). In addition, a new digital receiver system has been acquired that can obtain dual-polarization delay-Doppler images at resolutions as fine as 1.25 m/pixel, three times finer than Goldstone can transmit, in preparation for possible use of higher-resolution waveforms in the future.

With the new chirp/digital receiver system, it is now possible to spatially resolve NEAs ~30 m in diameter and estimate their 3D shapes. The chirp imaging system also enables finer precision ranging astrometry, particularly for tiny objects, with uncertainties of ~10 m.

Clones of the new digital receiver equipment were installed at Arecibo and Green Bank in 2014. Using Goldstone to transmit, Arecibo can now acquire images with a resolution of 3.75 m, which is twice as fine as Arecibo can achieve monostatically. The new equipment was successfully tested at Arecibo with observations of NEA 2014 HQ124 (**Figure 3**) in June 2014 and at Green Bank with observations of 2005 YQ96 and 2004 BL86 in January 2015. When used in bistatic mode with Goldstone transmitting and Arecibo receiving, the SNRs are about five times stronger relative to those obtainable with monostatic observations at Goldstone. Reception at Green Bank increases the SNRs by a factor of ~2 relative to monostatic observations due to Green Bank's larger diameter (100 m) and the doubling of the integration time.

Radar speckle tracking

Development of the radar speckle technique for estimation of asteroid spin vectors (Busch et al. 2010) is a major new capability since publication of *Asteroids III*. When illuminated with a monochromatic coherent uncoded radar waveform (continuous-wave or CW observations), each point on a target re-radiates with a random phase determined by its distance from the transmitter and the radar scattering properties of the surface. These wavefronts combine, producing a pattern of constructive and destructive interference that project onto Earth as high and low intensity splotches known as radar speckles. The speckles have a characteristic length scale of $L_{speckle} = D\lambda/d$, where D is the distance to the target, d is its diameter, and λ is the radar wavelength. For near-Earth asteroid radar targets, $L_{speckle}$ is usually >100 km and <10,000 km.

As the target rotates, the speckle pattern moves in the same direction as the target's surface. By tracking the speckle motion, it is possible to estimate the pole direction, sense of rotation, and rotation rate (Margot et al. 2007, 2012). For objects with unknown spin states, the antennas must be separated by less than the speckle scale (Busch et al. 2010). Near-Earth asteroids can be observed with speckle tracking by

transmitting from Arecibo or Goldstone and receiving with elements of the Very Long Baseline Array (VLBA) or Very Large Array (VLA).

The current discovery rate of near-Earth asteroids is ~1500 per year, of which ~5-10 are suitable for speckle tracking. This technique has been applied to a number of NEAs and has resolved spin state ambiguities for (341843) 2008 EV5 (Busch et al. 2011) and 2005 YU55 (Busch et al. 2012).

Shape modeling improvements

The 3D shape reconstruction software was originally written by R. S. Hudson (Hudson 1993) who used it to produce detailed shape models of contact binary 4769 Castalia (Hudson and Ostro 1994), non-principal axis rotator Toutatis (Hudson and Ostro 1995; Hudson et al. 2003), angular asteroid 6489 Golevka (Hudson et al. 2000), and less detailed models of several other NEAs.

When *Asteroids III* was published, the software was capable of handling 24 parameters describing the spin, shape, and reflectivity of asteroids, and 11 types of penalties designed to guide the optimization routine. Since then, Christopher Magri has overseen most of the development and maintenance of the software and documentation (Magri et al. 2007), with contributions from others starting in 2005 when the software was released more widely. The software is now more capable and easier to use. A number of graphical capabilities and penalty functions have been added, and the software can now handle a greater variety of input formats, coding schemes, and sampling modes. The modeling of photometric properties has also been significantly expanded. Ovoid shapes are now supported in addition to the original ellipsoid, spherical harmonic, and vertex shape representations. The user can also specify pixel masks to vignette one component of a binary asteroid when modeling the other component (Ostro et al. 2006) or to assign weights to different parts of an image (Nolan et al. 2013). The software can handle time-variable spin rates and spin impulses. The former was instrumental in establishing the first YORP detection (Taylor et al. 2007) and the latter is important in representing spin state changes during close planetary encounters (Takahashi et al. 2013). A libration model has also been incorporated to properly represent the dynamics of asteroid satellites (Naidu and Margot 2015). The current version allows for 243 adjustable parameters and 24 penalties to the objective function. This makes it a rather specialized tool with a substantial learning curve, but also an invaluable asset that has transformed the depth and breadth of asteroid radar data analysis.

Science Results since Asteroids III

1. Ground-truth of radar shape models by spacecraft missions: (25143)

Itokawa and (4179) Toutatis.

(25143) Itokawa

Itokawa was the first near-Earth asteroid visited by a spacecraft for which a 3D model from inversion of radar images was also available. Ostro et al. (2004) reported radar observations and a physical model from extensive imaging in 2001, and Ostro et al. (2005) incorporated additional radar images obtained in 2004 to estimate improved models.

The radar observations provided repeated coverage over a restricted range of longitudes in Itokawa's northern hemisphere in 2001 and sparse coverage of other longitudes on three days in 2004. Due to the nearly 12 h rotation period, radar images obtained in 2001 sampled very similar orientations day after day, although two weeks of sky motion ultimately extended the rotational coverage somewhat (see Fig. 1 from Ostro et al. 2005). The asteroid's pole direction and sky positions in 2001 precluded seeing the bend between Itokawa's "head" and "body." In 2004, the sky positions were very different and the concavity between the components was conspicuous. Unfortunately, in 2004 radar imaging occurred on far fewer days than in 2001, so a significant fraction of the surface was never seen at high resolution, and this propagated into limitations for the shape model. The highest range resolutions in 2001 and 2004 were 15 m/pixel at Arecibo and 19 m/pixel at Goldstone.

In 2005, the *Hayabusa* spacecraft began an extended encounter with Itokawa (Saito et al. 2006; see the chapters by Yoshikawa et al. and Scheeres et al. in this volume). The *Hayabusa* images reveal zeroth-order agreement with the Ostro et al. (2005) smooth model's shape and dimensions, but the spacecraft data also revealed obvious differences. **Figure 4** compares the 3D models estimated from the radar and spacecraft images. The Ostro et al. radar model has principal axes within 10% of 594 x 320 x 288 m. The dimensions reported by Saito et al. were 535 x 294 x 209 m with uncertainties of ~1 m. Thus, within their stated uncertainties, the long and intermediate axes are consistent but the short axis is not. The mismatch of the short axis is probably a consequence of significant gaps in latitude coverage in the radar images. The subradar latitudes during radar imaging were never within 45 degrees of the poles and they occurred over a relatively narrow range of longitudes.

Ostro et al.'s smooth model shows a bend between the head and body but it underestimated the depth of the neck, a discrepancy noted in the paper. In practice, during the modeling process it is often difficult to fit every feature visible in the images with the shape reconstruction algorithm currently in use. For example, the fits to the narrow end were not as tapered as indicated by the data from 2001 even though various approaches were attempted to improve them. The bend between the head and the body in the synthetic images reported by Ostro et al. is not as deep as it appears in the radar images. The shape modeling started with a single-component; in retrospect, the modeling could have produced better fits had it started with two overlapping ellipsoids (S. J. Ostro, pers. comm.), an approach that

was not in use in 2005. For example, Magri et al. (2011) started modeling deeply bifurcated contact binary (8567) 1996 HW1 with overlapping ellipsoids and obtained excellent fits. The radar model of Itokawa also has an equatorial ridge that is not present on the asteroid; this was noted by Ostro et al., and is probably an artifact due to the combination of penalties against rough or concave surfaces, and also due to the *Shape* software's default vertex adjustment order from south to north in a spiral pattern. The effects of the order of vertex adjustment were explored by modeling 2008 EV5 by Busch et al. (2011), who found that when the adjustment pattern was randomized, the sharpness of the equatorial ridge was reduced.

Boulders are ubiquitous in spacecraft images of Itokawa but were any visible in the radar data? Hints of small-scale topography at the resolution limit are visible in Arecibo images near the neck in an area where *Hayabusa* images show several decameter-scale boulders, but the resolution in the radar images was insufficient to make statements about the origin of the radar features. Yoshinodai, the largest boulder, was not visible due to gaps in the radar latitude and longitude coverage. Inspection of the 2001 radar images shows a cluster of radar-bright pixels corresponding to a ridge several tens of meters in extent in the spacecraft images of the northern hemisphere between the "head" and the broad smooth region known as Sagamihara.

(4179) Toutatis

Toutatis was imaged with radar during close Earth approaches in 1992, 1996, 2000, 2004, 2008, and 2012. Hudson and Ostro (1995) estimated the first 3D model of Toutatis using the 1992 images with a resolution of 75 m/pixel; Hudson et al. (2003) estimated a high-resolution model utilizing images from 1992 and 1996 with resolutions as fine as 18.75 m/pixel. The Hudson et al. (2003) high-resolution model is among the most detailed published to date.

Toutatis is the second asteroid imaged in detail by radar that has also been visited by a spacecraft, and it therefore provides an important "ground-truth" test of the shape modeling process (see also the chapter by Barucci et al. in this volume). The *Chang'e 2* spacecraft flew by Toutatis on 2012 Dec. 13 and acquired a series of images at resolutions as high as ~2 m/pixel. Due to the asteroid's slow rotation and the spacecraft's velocity, the *Chang'e 2* images show only one side.

Huang et al. (2013) and Zou et al. (2014) describe images obtained by the spacecraft and compare them with the Hudson et al. (2003) model. The *Chang'e 2* images match the asteroid's orientation as predicted by the radar-derived spin state model (Takahashi et al. 2013), and show many of the features in the radar-derived Toutatis shape model presented in Hudson et al. (2003): the large and small lobes of the asteroid, the neck between them, and ridgelines and depressions on both lobes (**Figure 5**). The spacecraft images yield estimates of the asteroid's dimensions that are consistent within their stated uncertainties: Hudson and Ostro (1995) reported

major axes within 0.1 km of 4.60 x 2.29 x 1.92 km; Huang et al. (2013) estimated "Toutatis' maximum physical length and width" to be within 10% of 4.75 x 1.95 km.

However, the *Chang'e 2* images also show mismatches that reflect limitations of early radar shape modeling techniques and of the 1992 and 1996 Toutatis radar data. The most pronounced differences appear in the model's large end, which is more tapered than in spacecraft images, and the region between the two lobes, which is more angular in the *Chang'e 2* images. The differences at the wide end originate primarily because previous radar observations did not have detailed coverage of that region. Although Toutatis was observed with radar in 2000, 2004, and 2008, those observations were restricted to no more than four days during each apparition and did not achieve thorough coverage due to the asteroid's slow rotation.

The true structure of the neck between the small and large components is more angular than in the Hudson et al. (2003) shape model. This is partly an artifact of the fitting procedure: the Hudson et al. shape model was rendered as a single surface, with a penalty function incorporated in the shape inversion that favored smooth shapes to prevent fitting noise. In this case, that procedure smoothed over real structure. Better results could have been obtained by using a two-component shape model, one for each of the two lobes, and by having higher-resolution radar data. Hudson et al. (2003) adopted a conservative modeling approach and stated "In penalizing relief in our shape reconstruction, we chose to suppress features rather than to risk showing features that might not be present on Toutatis." Although the match between the Hudson et al. shape model and Toutatis' shape as seen by *Chang'e 2* is not perfect, it validates the use of radar shape modeling in understanding asteroid shapes and spin states.

During the 2012 encounter, Toutatis was imaged with radar at resolutions up to 3.75 m/pixel, the highest resolution radar images ever obtained for this object. The images placed tens of thousands of pixels on the asteroid, covered the wide end more extensively than previously, and revealed a number of small radar-bright spots that Busch et al. (in prep.) linked with boulders in the *Chang'e 2* images.

Propagation of Toutatis' spin vector from 1992 to 1996 and 2000 showed orientation differences that were within the uncertainties of the Hudson and Ostro (1995) spin state, but images obtained in 2004 and 2008 clearly revealed discrepancies that were much larger. Takahashi et al. (2013) fit the images using an updated model for the shape and spin state that incorporated radar images obtained through 2008 and integrations that explicitly included gravitational perturbations experienced by Toutatis throughout its heliocentric orbit. They were able to successfully reproduce the orientation during each apparition imaged by radar. They found that the spin state changed during each flyby with the most pronounced changes occurring during the closest encounter within 0.01 au (~4 lunar distances) in 2004. This is one of the first instances where changes to a near-Earth asteroid's spin state during close Earth flybys have been detected. Similar changes are likely

to become evident for an increasing number of NEAs as future radar observations occur; for example, Scheeres et al. (2005) predicted that spin state changes should be obvious with (99942) Apophis after its approach within 5.1 Earth radii in 2029.

Main-belt Asteroids

Many main-belt asteroids (MBAs) have been observed with radar since publication of *Asteroids III*, but less work has been done with this population because far fewer MBAs are suitable for detailed imaging and the SNRs of the best targets are much lower than they are for NEAs. Most MBAs observed recently have been CW detections at moderate to weak SNRs and all have been at Arecibo. However, a number of main-belt asteroids have been imaged, most notably (4) Vesta, (5) Astraea, (7) Iris, (12) Victoria, (216) Kleopatra, and (654) Zelinda. In principle, Arecibo is so sensitive that several main-belt asteroids could be detected with radar on any night of the year.

Magri et al. (2007) presented detailed statistical analyses of the radar albedo and circular polarization ratio at 12.6 cm wavelength of 84 MBAs, 55 of which were observed by radar for the first time. Some conclusions from an earlier study (with a smaller sample size) by Magri et al. (1999) were strengthened: M asteroids have higher mean radar albedos and a wider range of albedos than other MBAs, suggesting that both metal-rich and metal-poor M-class objects exist; C- and S-class MBAs have indistinguishable radar albedo distributions; and the F, G, P, and D classes are not as radar-bright as C and S objects (but a convincing statistical test requires larger sample sizes). In contrast with earlier work, Magri et al. (2007) found that S-class MBAs have higher circular polarization ratios at 12.6 cm wavelength than other MBAs, indicating greater near-surface structural complexity at decimeter scales.

Shepard et al. (2008a, 2011) report that circular polarization ratios at 12.6 cm wavelength for E-class main-belt asteroids (44) Nysa, (64) Angelina, (434) Hungaria are significantly higher than for most other taxonomic classes but somewhat lower than the polarization ratios reported among E-class near-Earth asteroids (Benner et al. 2008). The E-class MBAs are up to several tens of km in diameter, so the difference in the circular polarization ratios relative to those seen among NEAs suggests that the circular polarization ratio has an inverse gravitational dependence.

Shepard et al. (2008b, 2010, 2011, 2014) estimated radar albedos for most of the X- and M-class MBAs that are detectable at Arecibo. This indicated high radar albedos for (16) Psyche, Kleopatra, (758) Mancunia, and (785) Zwetana, suggesting that they are almost certainly metallic; established evidence for wide variations in radar albedo as a function of rotation on Psyche, (129) Antigone, (135) Hertha, Mancunia, and Zwetana; suggested deep concavities on numerous objects; and showed that more than 60% of M-class asteroids with 3 μm hydration features reported from

infrared spectroscopic observations (Rivkin et al. 2000) have high radar albedos that are consistent with largely metallic surfaces. The presence of hydration features associated with these M-class asteroids is puzzling; Shepard et al. (2014) suggest that these may be the results of material delivered via impacts. Variations in the radar albedos also suggest compositional and/or structural complexity on large scales (Shepard et al. 2014).

(21) Lutetia
Shepard et al. (2008) reported delay-Doppler images of Lutetia prior to the Rosetta flyby in 2010. The images viewed Lutetia along the polar axis and were not sufficient for 3D shape estimation, but they suggested a polar dimension of 84 +- 12 km that was consistent with later observations by the *Rosetta* spacecraft (Sierks et al. 2011; see the chapter by Barucci et al. in this volume).

(7) Iris
Arecibo radar images of Iris obtained in November 2006 reveal a topographically complex object whose gross shape is approximately ellipsoidal with equatorial dimensions within 15% of 253 x 228 km (Ostro et al. 2010). The most prominent features are three ~50-km-diameter concavities almost equally spaced in longitude around the south pole that are probably impact craters.

(216) Kleopatra
Kleopatra has been observed at Arecibo in 1999 (Ostro et al. 2000), 2008, and 2013. The 2008 and 2013 delay-Doppler images confirm the "dogbone" shape reported by Ostro et al. (2000) but hint that the radar albedo may be somewhat lower than previously reported. The shape reported by Ostro et al. (2000) has been confirmed by adaptive optics imaging reported by Descamps et al. (2011) who also discovered that Kleopatra has two small moons. The SNRs of the radar observations spatially resolve the primary but are not strong enough to reveal echoes from the satellites. Additional information about Kleopatra appears in the chapter by Scheeres et al. in this volume.

Yarkovsky effect detections enabled by radar astrometry
The Yarkovsky effect is a key mechanism for the delivery of NEAs from the main belt to the near-Earth region and it has been the subject of extensive theoretical investigations (Bottke et al. 2002, 2006). A description of the Yarkovsky effect appears in the chapter by Vokrouhlicky et al. in this volume so here we will concentrate on the role that radar can play in its detection and the implications it has for constraining the physical properties of NEAs.

Radar observations of NEAs provide important opportunities to measure the Yarkovsky orbital drift. This effect has been detected with Arecibo radar data for (6489) Golevka (Chesley et al. 2003) and is the dominant source of uncertainty in some near-Earth asteroid trajectory predictions (Giorgini et al. 2002, Farnocchia et al. 2013) for bodies smaller than ~2 km. The Yarkovsky effect acts on the semi-

major axis linearly with time and the mean anomaly quadratically with time as a function of an object's spin, shape, thermal inertia, other material properties, and orbit. For asteroids of known sizes and spins, a measurement of the Yarkovsky drift rate can be interpreted in terms of bulk density and thermal inertia (Chesley et al. 2003, Nugent et al. 2012). If independent measurements of the thermal inertia exist, then it is possible to estimate the bulk density of the object (Chesley et al. 2014) and thus constrain its internal structure. Although the Yarkovsky drift can be estimated in some cases with optical astrometry alone (Nugent et al. 2012, Farnocchia et al. 2013), the uncertainties associated with these orbital drift determinations are typically reduced by an order of magnitude when radar data are included.

Giorgini et al. (2002) established the long-term coupling between the orbital evolution of (29075) 1950 DA (and NEAs in general) and physical properties such as spin state, shape, thermal inertia, and bulk density through the action of the Yarkovsky effect. The Yarkovsky effect is a major source of uncertainty for the future motion of Apophis (Giorgini et al. 2008) and Bennu (Chesley et al. 2014) and can lead to resonant returns and potential Earth impacts via deflection through keyholes.

Vokrouhlicky et al. (2000) predicted that the Yarkovsky effect could be detected for several NEAs with future radar ranging measurements. This was confirmed by Chesley et al. (2003) for Golevka through a combination of Arecibo and Goldstone radar astrometry obtained in 1991, 1995, and 2003, and utilization of the 3D model published by Hudson et al. (2000). This yielded a bulk density of 2.7 g/cm^3 and was the first detection of the Yarkovsky effect for a solar system object. Predictions for detecting the Yarkovsky effect for other NEAs appeared in Vokrouhlicky et al. (2005a, 2005b). In general, three radar detections spread out over at least several years are necessary, although due to the dependence on the mass, a longer baseline may be required for more massive objects and a shorter baseline could suffice for smaller ones.

Chesley et al. (2014) report a Yarkovsky effect detection for (101955) Bennu based on a weak ranging detection at Arecibo in 2011 coupled with radar astrometry obtained in 1999 and 2005 (Nolan et al. 2013). The thermal inertia was already available (Emery et al. 2013), enabling direct estimation of the asteroid's mass and bulk density, information that is invaluable for the *OSIRIS-Rex* mission that will arrive at Bennu in 2018.

Vokrouhlicky et al. (2005b) described binary NEAs for which detection of the Yarkovsky effect could soon be possible. Masses of binary systems can be estimated by fitting range-Doppler measurements between the components of binary system and application of Kepler's third law (Margot et al. 2002), so a Yarkovsky effect detection enables estimating the mass from an independent technique (although one that often requires numerous assumptions and is less robust than direct fitting of the mutual orbit of a binary system). The first binary where both approaches

provided mass estimates is 1862 Apollo, whose bulk density estimated from the orbit of ~2.6 g/cm^3 (T. Ford, pers. comm.) is consistent (to within the uncertainties) with the value of 2.86 +0.48 -0.68 g/cm^3 estimated by Rozitis et al. (2013) from the Yarkovsky effect detection (Farnocchia et al. 2013a).

To facilitate future Yarkovsky effect detections, NEAs previously detected by radar are now observed at every opportunity when the SNRs are expected to be strong enough for ranging measurements. During the coming decade, this could increase the number of NEA mass and bulk density estimates by a factor of several. Among these is 99942 Apophis, which will approach within 0.113 au in 2021, when radar astrometry is likely to yield a strong Yarkovsky effect detection and estimates of the asteroid's shape, mass, and density (Giorgini et al. 2008; Farnocchia et al. 2014).

Radar detection of the YORP effect: **54509 YORP**

The YORP effect is a torque on the spin state of an asteroid due to the absorption and anisotropic re-emission of sunlight (Rubincam 2000; see also the chapter by Vokrouhlicky et al. in this volume). The first direct evidence of the YORP effect came from combined radar and optical observations of asteroid (54509 YORP) (Taylor et al. 2007; Lowry et al. 2007), and optical observations of 1862 Apollo (Kaasalainen et al. 2007).

By virtue of its nearly 1:1 orbital resonance with Earth and a moderate heliocentric eccentricity, asteroid YORP made annual close approaches to Earth from 2001 to 2005. In 2001, Goldstone images and optical lightcurves established a rapid rotation period of 12.2 minutes. Additional lightcurves were obtained annually, as were radar observations at Arecibo in 2004 and 2005. Under the assumption of an unchanging spin state, neither the radar images from 2001 and 2004 nor the lightcurves from 2001 to 2005 could be linked self-consistently. Combining the radar-derived spin-axis orientation with the optical data showed clear evidence for a discrete change in the sidereal spin period from year-to-year (Lowry et al. 2007), and applying the three-dimensional shape model from inversion of the radar images revealed that a continuously increasing correction to the rotational phase was required to simultaneously fit the lightcurves over multiple years (Taylor et al. 2007). Both methods revealed a change in spin rate of (2.0+- 0.2) x 10^{-4} deg/day^2, amounting to more than a 200 deg of drift in rotation phase when trying to link lightcurves obtained over 4 years. The observation of YORP accelerations on the rotations of objects spanning from 100-m-sized asteroid YORP to multi-km NEA (1620) Geographos (Durech et al. 2008) suggests that the YORP effect is capable of altering the spin of most near-Earth asteroids. Furthermore, the YORP effect is mass dependent, and if detected, it can provide a useful constraint on an asteroid's mass (Capek and Vokrouhlicky 2004).

(99942) Apophis

When discovered in December of 2004, Apophis was briefly estimated to have a 2.7% chance of impacting the Earth in 2029. Additional optical measurements quickly showed there was no impact risk at that time. However, there will be an extremely close approach to the Earth in 2029, estimated to be a 1 in 800 year event for an object of that size.

Arecibo subsequently detected Apophis at distances of 0.192-0.268 au in 2005 and 2006, with CW echo power spectra and ranging (Giorgini et al. 2008). The first radar echoes acquired on January 27, 2005, were 4.8-sigma off the frequency predicted by the optical-only solution. Including the radar measurements in a new orbit solution revealed a 1.4 arcsecond systematic bias in the pre-discovery optical measurements and moved the April 13, 2029 encounter prediction 4.4 Earth radii closer to Earth while reducing the uncertainty in Apophis' location during the encounter by 98%. This was a five-sigma trajectory correction.

The new radar-corrected orbit had better predictability through the 2029 encounter, but degraded rapidly thereafter. This was due to the new solution's deeper entry into the Earth's gravity field in 2029, an approach 45% closer than predicted prior to the debiasing enabled by radar observations. The steeper gravity gradient differentially pulls on and elongates the statistical uncertainty space to a greater extent than the more distant uncorrected pre-radar encounter.

Echo power spectra, ranging measurements, and coarse-resolution images of Apophis were obtained at Goldstone and Arecibo from December 2012 through March 2013. The images and echo bandwidths suggest an elongated object but are insufficient for estimation of a detailed 3D model. There had been some potential for the Yarkovsky effect to be detected if Apophis was on the low-mass side of what was possible, with a spin pole perpendicular to its orbit plane, in concert with favorable thermal properties. However, the new radar astrometry excluded that extreme combination of properties, showing no significant evidence of Yarkovsky effect motion over 2004-2013 (as predicted by Farnocchia et al. 2013b), and effectively ruled out the remaining impact potential in 2036. Reliable orbit prediction is now possible into the 2060s but the orbital uncertainties grow rapidly afterward.

NEA Population trends

Overview of the NEA Shape and Spin Distributions

Radar observations of near-Earth asteroids have revealed a heterogeneous population with a wide range of shapes and spin characteristics. NEAs detected by radar range over roughly four orders of magnitude in size from meter-scale objects 2006 RH120 and 2013 EC20 to the largest NEA, (1036) Ganymed, at over 30 km in effective diameter. Their rotation periods span at least four orders of magnitude as well, from 16 seconds to more than one week. The radar-determined shapes of NEAs are similarly diverse, from simple spheroids and ellipsoids to multiple-

component (binary and triple) systems to double-lobed contact binaries and extremely irregular angular bodies.

Taylor et al. (2012) examined the shape and spin distributions of the NEA population observed with the Arecibo radar system since 1998. They found that radar-observed NEAs with diameters larger than ~200 m (with a sample size of over 100 objects) are not dominated by a single category of shape. A radar-observed multiplicity fraction of ~17% among near-Earth asteroids with H < 21 is in agreement with optical observations (Pravec et al., 2006; see also chapter by Margot et al. in this volume), while, perhaps surprisingly, contact binaries account for a similar fraction at ~14%, roughly 50% larger than reported in earlier estimates (Benner et al. 2006). At smaller sizes, binaries and contact binaries are much less common with only three binaries and one contact binary known with H > 21 and none with H > 22. Further, only about one in four objects with H > 21 are assigned basic shapes due to the difficulty in obtaining sufficient resolution in radar images. Those with shapes assigned often appear irregular either with angular shapes or highly specular reflections from facets.

The spin distribution of near-Earth asteroids estimated from radar observations closely matches the spin distribution determined from optical lightcurves (**Figure 6;** see the chapter by Scheeres et al. in this volume for a different version of this figure). Lightcurves are biased against small, slowly rotating bodies because of their inherent faintness, which often limits their observability and hence the opportunity to confidently record an entire rotation period on the scale of many tens of hours. Radar observations detect an apparent spin rate based on the instantaneous echo bandwidth, which does not require one to observe an entire rotation. Thus, radar should detect a small, slowly rotating body as a narrow echo.

The distinct change in the shape and spin distributions of the near-Earth asteroid population at H of 21 or 22 (100- to 200-m diameters) may indicate fundamental structural changes at this scale.

Abundance of contact binary NEAs

Radar imaging since completion of the upgrade at Arecibo in 1999 revealed more than thirty NEAs that are deeply bifurcated (Benner et al. 2006, Brozovic et al. 2010, Magri et al. 2011). Benner et al. (2006) found that at least ~10% of NEAs > 200 m in diameter are candidate contact binaries, where a contact binary is defined as "an asteroid consisting of two lobes that are in contact, have a bimodal mass distribution, that may once have been separate." By this definition, objects such as Itokawa and Toutatis that have two components with substantial size differences, and thus lack bimodal mass distributions, were not classified as contact binaries. The definition of a contact binary is necessarily subjective, and due to considerable subsequent research on the formation and evolution of Itokawa and radar imaging of hundreds of additional NEAs, we now relax the definition to include objects that are obviously bifurcated, have components that can be significantly different in size

(with size ratios of at least 4:1), and mass distributions that aren't bimodal. With this revised definition, the fraction of candidate contact binaries imaged by radar has grown to ~14% (Taylor et al. 2012). Given that true binaries comprise ~16% of the NEA population above ~200 m in diameter (Margot et al. 2002), this implies that the abundances of contact binaries and true binaries are comparable and that these objects together constitute ~30% of the NEA population > 200 m in diameter. **Figure 7** shows an example: the 3D model of 1996 HW1, which was imaged at Arecibo in 2008 and is one of the most deeply bifurcated NEAs observed to date (Magri et al. 2011).

These contact binary objects display considerable dynamic range in long axis lengths, spectral classes, and spin states. The largest is (192642) 1999 RD32, with a long axis of ~6 km, and the smallest is 2013 JR28, with a long axis of ~100 m. The fastest rotator is (4769) Castalia with a rotation period of 4 h, and the slowest, 2002 FC and 2004 RF84, have unknown rotation periods of days to weeks. None of the contact binaries rotates as fast as the rapidly spinning primaries of most NEA binaries and triples (see the chapter by Margot et al.). Some of the contact binaries rotate at rates close to where they could separate if spun up slightly (Benner et al. 2006, Scheeres et al. 2007). A significant (but not yet quantified) fraction are non-principal axis rotators.

How did such objects form and why are they so abundant? Plausible formation mechanisms are by low-velocity collisions; collapse of true binaries through tidal friction or as a result of orbital perturbations during close planetary encounters; by spin-up due to YORP; or by partial disruption during close planetary flybys. Combinations of the factors above may be necessary to explain the slowest rotators.

Binary NEAs

Binary asteroids are a field of vigorous research and are treated in considerable detail by Margot et al. in this volume. In this chapter we mention them only to illustrate points that also apply to broader trends within the NEA population.

Equatorial Ridges

Evidence for equatorial bulges appears in radar images for many rapidly rotating NEAs > 200 m in diameter, some relatively slow rotators, and for most of the primaries in binary and triple NEA systems. The first clear case was the primary of binary (66391) 1999 KW4 (Ostro et al. 2006), which exhibited a "double exposure" appearance at its leading edge that corresponded to the sharp edge of its ridge. Bulges have since been seen in models for (311066) 2004 DC (Taylor 2009), 2008 EV5 (Busch et al. 2011), (136617) 1994 CC (Brozovic et al. 2011), 2005 YU55 (Busch et al. 2012), the primary of (185851) 2000 DP107 (Naidu et al. 2015), and in radar images for numerous other NEAs for which shape models are not yet available. **Figure 8** shows renderings of shape models for selected objects with

bulges. The ridges are thought to form via YORP-induced spin-up acting on an object with a rubble pile internal structure (Harris 2009, Walsh et al. 2009; see also the chapter on asteroid interiors by Scheeres et al. in this volume). Although no formal estimate of their abundance is available, radar observations and 3D modeling indicate that NEAs with equatorial ridges are relatively common. In more detail, the delay-Doppler signature of objects with oblate vs. spheroidal shapes are discussed by Busch et al. (2011) and applied to 2008 EV5.

In addition to the appearance of shape models, direct evidence for oblate shapes comes from images of 2013 WT44, which was observed at a subradar latitude close to a pole. **Figure 9** compares the radar images of 2013 WT44 with a high-latitude view of the 1999 KW4 Alpha model (Ostro et al. 2006) to illustrate the appearance of the equatorial ridge from a nearly pole-on perspective. The 2013 WT44 images show a flat polar region, a roughly cone-shaped hemisphere, and a "doubly-curved" trailing edge region (highlighted with arrows in the figure) that shows the entire circumference of an equatorial ridge tilted relative to the radar line-of-sight.

Radar evidence for impact craters

Features suggesting impact craters have been seen on numerous NEAs imaged by radar starting with Toutatis in 1992 (Ostro et al. 1995; see also Hudson et al. 2003). The candidate craters generally take the form of circular to ellipsoidal radar-dark features from tens of meters to more than 2 km in extent. Interpretation of radar-dark features is hampered by the counterintuitive nature of delay-Doppler images, the resolution, signal-to-noise ratios, and rotational coverage of the data. Deep concavities are visible along the leading edges of other objects, but do not appear as radar-dark regions. Concavities are also evident in some shape models and may represent craters but their origins are not clear. Candidate craters appear in radar images of many objects such as (4183) Cuno, (33342) 1998 WT24 (Busch et al. 2008), (53319) 1999 JM8 (Benner et al. 2002) and (185851) 2000 DP107 (Naidu et al. 2015). **Table 1** lists NEAs imaged by radar that show evidence for impact craters. **Figure 10** shows Arecibo images of (136849) 1998 CS1, which has a number of radar-dark features suggesting impact craters, and **Figure 2** shows images of 2005 YU55, which has several small ellipsoidal radar-dark regions and a small concavity on its leading edge. Craters are conspicuously absent in radar images of many other NEAs, perhaps because such features are not present, due to limited viewing geometry, or perhaps because the SNRs and resolution are insufficient.

Radar evidence for boulders on NEA surfaces

Delay-Doppler radar observations of numerous near-Earth asteroids have revealed many small clusters of radar-bright pixels in some of the highest signal-to-noise ratio images obtained at Arecibo and Goldstone. Many of the spots persist as the asteroids rotate, so the bright pixels are not receiver noise, self noise, or artifacts. Clusters of bright pixels appear primarily in high-resolution radar images with

resolutions of 4 - 19 m/pixel and suggest that these are features a few tens of meters in extent or smaller. Many spots appear near the trailing edges of the images and are up range from radar shadows, implying that the source for some of the features is small-scale topography. **Figures 2** and **3** show images of 2005 YU55 and 2014 HQ124, NEAs that have conspicuous and widespread radar-bright spots. To date, small groups of bright pixels have been seen on at least 14 NEAs, establishing that these features are relatively common.

Benner et al. (2014) suggest that the bright pixels are echoes from surface and near-surface boulders, which have also been seen on each of the three near-Earth asteroids imaged at close range by spacecraft: (433) Eros (*NEAR-Shoemaker*), Itokawa (*Hayabusa*), and Toutatis (*Chang'e 2*). These asteroids have also been imaged by radar, but the signal-to-noise ratios and/or resolutions were insufficient to reveal boulders with Eros and Itokawa. However, radar images of Toutatis obtained in 2012 reveal spots that can be linked with boulders in the *Chang'e 2* spacecraft images. Of the objects with evidence for boulders, 1999 RD32 is the largest, with a long axis of ~7 km, and 2014 BR57 is the smallest, with a diameter of about 80 m.

Circular polarization ratio correlations with spectral class

Benner et al. (2008) conducted a survey of more than 200 near-Earth asteroids detected by radar and found distinct correlations between their circular polarization ratios (abbreviated as "SC/OC") and some spectral classes. E- and V-class NEAs have high SC/OC values, a trend that is mirrored among the handful of E-class main-belt asteroids that have also been detected to date by radar (Shepard et al. 2008c, 2011). In contrast, SQ-class and optically dark NEAs show circular polarization ratios that vary from ~0.1 to ~0.5 but otherwise show no obvious trends. 56% of the NEAs in which SC/OC > 0.5 in the sample have unknown spectral classes, and if all of them turn out to be E- or V-class objects, that implies that EV-class NEAs are much more abundant in the near-Earth population than has been previously realized. Since the study by Benner et al. (2008) was published, the sample of NEAs observed by radar has more than doubled and the pattern of high SC/OC values among E- and V-class objects has persisted (Springmann et al. 2013).

How are we to understand these correlations? Benner et al. (2008) speculated that this could possibly "be due to the intrinsic mechanical properties of different mineralogical assemblages but also may reflect very different formation ages and collisional histories." The fact that the trend of high SC/OC appears to remain across a wide range of diameters, including inner MBAs up to several tens of km in diameter, suggests that there is at least a component due to composition.

Virkki et al. (2014) modeled the effects of electric permittivity and the size of surface structure on asteroid radar circular polarization ratios and radar albedos. They find that obtaining SC/OC > 1 at 3.5 and 13 cm wavelengths requires a high refractive index (n > 2), which may explain the high polarization ratios observed

among basaltic V-class objects because basalt has a relatively high refractive index. In general, SC/OC > 0.5 occurs from surfaces with scatterers from one to a few times larger than the radar wavelength, although this is also a function of the refractive index and thus composition. Fundamentally, though, asteroid surfaces with high SC/OC are still not well understood.

Results for Selected Asteroids

(101955) Bennu

Nolan et al. (2013) estimated the shape of Bennu based on Arecibo and Goldstone imaging in 1999 and 2005 (**Figure 11**). Bennu is an optically-dark spheroid with major axes of 565 x 535 x 508 m, a sidereal rotation period of 4.3 h, a modest equatorial ridge, evidence for a relatively large boulder in the southern hemisphere, and broad-scale near-surface roughness features.

Chesley et al. (2014) report detection of the Yarkovsky effect for Bennu through radar astrometry obtained in 1999, 2005, and 2011 and optical astrometry from 1999-2013. This yields an estimate of the mass and bulk density that are invaluable for planning the *OSIRIS-REx* mission. The density, $\rho = 1.3$ kg/m^3, implies a macroporosity of ~40% and suggests a rubble-pile internal structure. Bennu has one of the highest impact probabilities known, and, due to frequent close Earth encounters, will probably require orbital monitoring indefinitely (Milani et al. 2009).

Bennu is the target of the *OSIRIS-REx* mission that will provide a stringent test for the shape modeling process when the spacecraft arrives in October 2018.

(4660) Nereus

Nereus has been identified as a potential spacecraft target since its discovery because of the low ΔV required for a rendezvous. Nereus was an early target for the *Near-Earth Asteroid Rendezvous* (*NEAR*) mission and the original target for the *Hayabusa* mission. Arecibo and Goldstone images of Nereus obtained in 2002 enabled Brozovic et al. (2009) to reconstruct a 3D model, which resembles an ellipsoid with principal axis dimensions X=510±20 m, Y=330±20 m and Z= 241^{+80}_{-10} m, and features two prominent facets.

(214869) 2007 PA8

Goldstone imaged 2007 PA8 on sixteen days in 2012. The images achieved range resolutions as fine as 3.75 m, placed thousands of pixels on the asteroid, and revealed an elongated, asymmetric object (**Figure 12**; Brozovic et al. in prep.). The surface has angularities, facets, and a concavity >200 m in diameter. Shape

modeling yields an effective diameter of 1.35 ± 0.05 km, and elongation (long/intermediate axis ratio) = 1.4. The modeling revealed that 2007 PA8 is a non-principal axis (NPA) rotator in short-axis mode with an average period of precession by the long axis around the angular momentum vector of 4.26 ± 0.02 days and an oscillatory period around the long axis of 20.55 ± 3.75 days. The amplitude of rolling around the long axis is 42 ± 7 deg. 2007 PA8 is the second confirmed short-axis mode NPA rotator found in the near-Earth asteroid population, after Apophis (Pravec et al. 2014).

(162421) 2000 ET70

Arecibo images of 2000 ET70 place thousands of pixels on the object (**Figure 13**, Naidu et al. 2013). The 3D physical model has dimensions of 2.6 x 2.2 x 2.1 km, a retrograde spin state with a 9 h period, and an unusually low optical albedo of ~2%. The northern hemisphere has dramatic ridges oriented approximately perpendicular to the long axis, but the southern hemisphere is much more rounded, a global shape dichotomy that is uncommon among NEAs imaged by radar to date.

(308635) 2005 YU55

2005 YU55 approached within 0.0022 au (0.85 lunar distances) in November 2011, the closest approach of a known asteroid >300 m in diameter since 1982 (2012 TY52) and until 2028 (2001 WN5). This provided an extraordinary opportunity for radar imaging and extensive observations were obtained at Goldstone, Arecibo, the Green Bank Telescope, and elements of the Very Long Baseline Array over two weeks (Busch et al. 2012). The signal-to-noise ratios were among the highest ever obtained for any near-Earth asteroid and resulted in radar images with resolutions as fine as 3.75 m in range (**Figure 2**). The images reveal a rounded object whose surface has many small radar-bright spots, suggesting numerous boulders, and radar-dark regions that may be impact craters. Modeling indicates that the shape is close to spheroidal with maximum dimensions of 360 ± 40 m in all directions. The shape has a ridge roughly parallel to the equator that resembles ridges seen on other rapidly-rotating spheroidal NEAs imaged by radar, but unlike those other objects, 2005 YU55 is a slow rotator with a period of ~19 h.

.

2014 HQ124

Bistatic Goldstone-Arecibo X-band images of 2014 HQ124 achieve a resolution of 3.75 m x 0.00625 Hz **(Figure 3)** and provide some of the most detailed radar views obtained for any near-Earth object (Benner et al. 2014). 2014 HQ124 is a slowly-rotating object that is elongated, bifurcated, and angular with a long axis of at least 400 m. The larger lobe has a narrow, sinuous, ~100-m-long radar-dark feature that may be a scarp or perhaps a fault. These observations were the first test of new data-taking equipment at Arecibo that can acquire images at 3.75 m resolution using transmissions from Goldstone. Radar astrometry increased the interval of reliable Earth encounter predictability by a factor of two to ~900 years.

(341843) 2008 EV5

Busch et al. (2011) observed 2008 EV5 with Arecibo, Goldstone, and the Very Long Baseline Array during the asteroid's passage within 0.022 au in December 2008. Radar speckle tracking indicates retrograde rotation; this is the first NEA where that technique was used successfully. The object has a diameter of 400 +- 50 m, a prominent ridge parallel to its equator, and a concavity about 150 m in diameter (**Figure 8**). The concavity may be an impact crater; if so, then its ejecta may have produced some of the numerous boulders that are suggested by radar bright spots near the south pole. This object was the target for the proposed European Space Agency's *Marco Polo-R* mission and is a leading candidate for NASA's proposed *Asteroid Redirect Mission.*

(33342) 1998 WT24

1998 WT24 approached within five lunar distances (0.0125 au) in December 2001, when it was the strongest asteroid radar target ever observed up to that point. This asteroid was observed extensively at Goldstone and Arecibo and yielded a detailed 3D model (Busch et al. 2008). The images show a rounded object with a conspicuous radar-bright spot several pixels in extent that persists over multiple rotations. The asteroid has a diameter of 415+-40 m and the shape is dominated by three large basins that may be impact craters.

(29075) 1950 DA

1950 DA is a type case highlighting the importance of radar astrometry and shape modeling for predicting asteroid trajectories and the interaction between orbits, shapes, and spin states due to the Yarkovsky effect.

1950 DA was discovered in 1950, lost until 2000, and then observed extensively at Arecibo and Goldstone during a close approach in March 2001. Radar astrometry indicated that 1950 DA will approach Earth in 2880, the outcome of which depends on the magnitude and direction of the Yarkovsky acceleration. Due to the uncertainties in unmeasured physical parameters, Giorgini et al. (2002) included uncertainties in the Earth impact probability by expressing it as an interval, concluding that "the maximum probability of impact is best expressed as being between 0 and 0.33%."

Shape modeling by Busch et al. (2007) generated two pole solutions and two corresponding shapes: one that is roughly spheroidal and ~1.2 km in diameter, and a second that is oblate, ~1.2 km from pole to pole, and ~1.6 km across at the equator (Busch et al. 2007). The data were insufficient to determine if 1950 DA spins prograde or retrograde, producing an ambiguity in the asteroid's future trajectory and thus in the impact probability.

Farnocchia and Chesley (2014) utilized additional optical astrometry, re-measured radar astrometry from 2001, and new radar ranging from Arecibo in 2012 to further improve the orbit. The main source of uncertainty remains the Yarkovsky effect, which was detected at the ~5σ level. Utilizing a statistical model of the Yarkovsky effect, they found that, due to the sign of the orbital drift, prograde rotation is ruled out. This appears to be the first time that a pole direction ambiguity has been resolved by detection of the Yarkovsky effect, which was predicted by Busch et al. (2007).

Rozitis et al. (2014) adopted the retrograde shape model from Busch et al. (2007) and used thermal modeling of *WISE* spacecraft data to estimate 1950 DA's thermal inertia and bulk density. They state that the asteroid's rapid spin (2.1 h) implies a need for cohesive forces to prevent rotational breakup. Rozitis et al.'s work hinges on the 5σ Yarkovsky effect detection reported by Farnocchia and Chesley (2014) and on the retrograde shape model without regard to the uncertainties in that model. However, more recently Hirabayashi and Scheeres (2015) find that cohesion is necessary over a much wider range of densities, indicating that a change in density estimate will not substantively impact the main conclusions of Rozitis et al. (see the chapter by Scheeres et al. in this volume).

Future radar and optical astrometry can refine estimates of 1950 DA's Yarkovsky effect drift, improve estimates of the asteroid's future trajectory, and improve estimates of its bulk density and constraints on its internal structure. The next opportunity for radar observations of 1950 DA is in 2032 when an extensive imaging campaign at Arecibo and Goldstone could provide higher resolution images than were obtained in 2001.

(1580) Betulia

Magri et al. (2007) modeled the shape and spin state of Betulia using Arecibo data obtained in 2002 and lightcurves obtained in 1976 and 1989. They obtain a model that resembles the Kaasalainen et al. (2002) convex-definite shape reconstructed from lightcurves but is dominated by a prominent concavity in the southern hemisphere. Betulia has an effective diameter of 5.39+-0.54 km and a shape that is roughly triangular when viewed along its polar axis.

(100085) 1992 UY4

Goldstone and Arecibo radar images of 1992 UY4 obtained in 2005 reveal a lumpy, modestly asymmetric, 2 km-diameter object. The surface is characterized by gently undulating topography with many modest concavities. Numerous fine-scale, radar-bright features are evident at the trailing edges and limbs; one of the most prominent has a visible extent of about 100 m and juts out abruptly from the approaching limb, suggesting a large block similar to the boulder Yoshinodai seen on 25143 Itokawa by the Hayabusa spacecraft (Saito et al. 2006).

Tiny Near-Earth Asteroids

Near-Earth asteroids with diameters < 140 m (corresponding to H > 22) comprise ~1/4 of all NEAs observed with radar. The fraction of such objects observed by radar has increased ~50% since publication of *Asteroids III* because more of these objects are being discovered with sufficient advance notice to schedule radar observations, due to greater access to telescope time, and due to more rapid response protocols. Several have been observed within one lunar distance, and one, 2006 RH120, was a temporarily captured satellite of Earth. A further motivation has been acute interest since 2011 in tiny NEAs that could be targets for human missions. To that end, as many objects on the NASA Near-Earth Object Human Spaceflight Accessible Targets Study list (NHATS; http://neo.jpl.nasa.gov/nhats/) are observed with radar as possible even if the SNRs are very weak.

Due to development of the 3.75 m resolution imaging system at Goldstone, it has become possible to obtain delay-Doppler images that can spatially resolve NEAs as small as ~30 m in diameter. This opens up a new capability to investigate the physical properties of a much smaller subset of the NEA population than was previously possible. The first object imaged at 4-m resolution was 2010 AL30 (Slade et al. 2010). More recently, several NEAs such as (367943) Duende (2012 DA14), 2013 ET, and 2014 BR57 have been imaged, revealing a suite of irregular to spheroidal shapes (**Figure 14**).

Ranging astrometry from tiny NEAs can yield orbits with sufficient precision to detect non-gravitational perturbations from solar radiation pressure. If detected, this perturbation yields an estimate of the area/mass ratio. To date, solar radiation pressure perturbations have been detected in the motion of one NEA observed by radar: 2006 RH120 in 2007 (P. W. Chodas, pers. comm).

The Future

The future for asteroid radar observations is potentially very bright if capabilities at least equal to those currently available at Arecibo and Goldstone are maintained. As the number of NEAs discovered has grown rapidly in the last decade, so too have the number of short-term targets-of-opportunity and targets known well in advance. This trend will only continue as existing surveys upgrade and as new surveys begin.

The Large Synoptic Survey Telescope (LSST) could yield vastly more NEA discoveries when it begins routine operations in the 2020s, and with it could come a dramatic increase in radar targets. Due to its sensitivity, it seems likely that many NEAs larger than a few tens of meters in diameter found by LSST will be discovered months or even years before they will be detectable by radar.

The number of NEAs observed annually with radar is a fraction of what could be done if a dedicated radar facility were available. Currently, among objects known in advance, most NEAs are scheduled with SNR larger than ~15/day at Arecibo and ~30/day at Goldstone. Schedules and equipment problems continue to be obstacles for observing on short notice but are less cumbersome than only a few years ago. The net effect is that roughly 1/3 of NEAs that are potentially detectable with radar are actually being observed.

Arecibo could observe many more asteroids if additional telescope time and funding were available. The observatory is already operating the S-band radar at close to the legal limit imposed by local air pollution laws and a significant increase would require new, lower-emission generators. Due to its extraordinary sensitivity, though, the most effective way to increase the number of NEA radar detections is to augment the number of observations at Arecibo.

Demand at Goldstone for spacecraft communications is expected to diminish over the next several years as existing spacecraft cease operations and as future spacecraft switch to NASA's 34 m antennas for tracking. This could provide an opportunity to observe significantly more asteroids. Although most requests at Goldstone to observe NEAs known well in advance are scheduled, obtaining time on short notice remains challenging because schedules for flight projects are arranged many weeks in advance, and changing schedules on short notice has effects that ripple through the DSN.

Other Radar Facilities

Are there other existing radar facilities that could be utilized to observe near-Earth asteroids? The 70 m Evpatoria antenna in Crimea has conducted bistatic NEA radar observations utilizing radio telescopes at Effelsberg (Germany), Medicina (Italy), and Irbene (Latvia) as receivers. Evpatoria has also acted as a receiver for Goldstone X-band transmissions of Golevka (Zaitsev et al. 1997), 1998 WT24 (Di Martino et al. 2004), and 2004 XP14 and could be used for monostatic observations of very close targets if the system were modernized (B. Shustov, pers. comm.). Installation of a high-power planetary radar was considered for the new 64 m Sardinia Radio Telescope (Saba et al. 2005) but was not implemented due to the cost.

In February 2013, J. Vierenen (pers. comm.) detected radar echoes from Duende with the EISCAT facility near Tromso, Norway; this was the first time EISCAT was used for asteroid observations. Nechaeva et al. (2013) observed Duende by using Evpatoria to transmit and Irbene and Medicina to receive. The 37 m X-band and 46 m UHF antennas at Haystack Observatory also detected Duende (P. Erickson and M. Hecht, pers. comm.). Radar observations of Duende were scheduled at the 35 m TIRA facility in Germany but those observations were cancelled due to logistical problems (D. Koschny, pers. comm.). Although orders of magnitude less sensitive

than Goldstone, these facilities could detect a modest number of near-Earth objects annually during very close flybys.

Future radar capabilities

A new radar facility began operations in January 2015 on the 34 m DSS-13 antenna at the Goldstone Deep Space Communications Complex. DSS-13 is an experimental test bed that has been equipped with an 80 kW klystron that transmits at C-band (7190 MHz, 4.2 cm). The klystron has a bandwidth of 80 MHz and can achieve a range resolution of up to 1.875 m/pixel that is twice as fine as the highest resolution at the 70 m DSS-14 Goldstone antenna and four times finer than at Arecibo. DSS-13 is not equipped to receive its own radar echoes, so reception must occur at another facility such as Green Bank, Arecibo, or the 34 m DSS-28 antenna at Goldstone. Bistatic DSS-13/Arecibo and DSS-13/Green Bank observations are significantly less sensitive than observations at DSS-14, but for very strong targets such as 2005 YU55, Duende, and 2014 HQ124, where the SNR is not a limiting factor, DSS-13 would have been ideal. The new radar at DSS-13 is in its commissioning phase and routine operations are planned by the end of 2015.

The 70 m DSS-43 antenna at the Canberra Deep Space Communication Complex in Australia and the 64 m Parkes Radio Telescope could in principle be configured as a bistatic radar system using an existing S-band transmitter on DSS-43 that can radiate 400 kW. This bistatic system might achieve SNRs perhaps ~4% as strong as those at Goldstone and could enable radar observations of very close NEAs at southern declinations that are inaccessible to Goldstone and Arecibo. Proof-of concept tests are planned in late 2015. Farther into the future, one of the 34 m Deep Space Network antennas at Canberra could be equipped with an 80 kW, 80 MHz klystron and transmitter identical to the system at DSS-13 (Davarian 2011).

Another concept in the early stages of development is the Ka-Band Objects Observations and Monitoring (KaBOOM) phased-array radar test bed at the Kennedy Space Center (http://www.nasa.gov/directorates/heo/scan/engineering/technology/KaBOOM.html). KaBOOM is a three-element array with antennas 12 m in diameter. The effective radiated power of an array of transmitters is proportional to N^2, where N is the number of array elements (Davarian 2011), so in principle it is possible use a large number of small antennas radiating low power (~5 kW) to achieve much higher sensitivity than with a single, large dish. The engineering challenges are formidable and it is not yet known if this technique is feasible.

Greater automation

Observing NEAs with radar remains a labor-intensive process that requires at least three people at the observatory to operate the telescope, transmitter, adjust cables, take data, make key decisions, and update ephemerides. At Arecibo it is still necessary to switch cables and adjust voltage gains when changing setups, a process that in principle could be automated with one electronics box. In the future, one can

envision a situation with a nightly queue where the telescope automatically moves from target to target, where software automatically processes the data to determine when a detection has occurred, estimates and reports range-Doppler corrections to the ephemerides, and then slews to the next target. Imaging of high-SNR targets would require more direct human control to maximize the scientific return, but weaker targets could be observed in the automated manner described above.

Shape Modeling

The shape models discussed above demonstrate a clear need for improvements to the shape modeling procedure. A better estimation algorithm that can fit topographically rugged objects is particularly desirable because features are often visible in radar images that the fits do not adequately reproduce. It would be helpful if a straightforward method of manually adjusting specific vertices on a model were possible in order to fit fine-scale features. Coupled estimation of the shapes and orbits of binaries would also be helpful.

Although increasing computer speed is useful, the limiting factor for estimating 3D models is actually the ability of the user to assess the fits. Experience has shown that the human eye is more reliable than the chi-square statistic for assessing the quality of fits, but this requires time-consuming visual inspection of many images.

Another impediment for augmenting the number of asteroid shape models is the paucity of near-Earth asteroid pole directions. Knowledge of the pole direction dramatically shrinks the time to estimate 3D shapes. Otherwise, pole estimation requires a lengthy grid search may that not yield a unique solution. Radar speckle observations can provide pole directions for the subset of targets with very strong SNRs, and increasing the number of days of radar observations to extend sky motion can help, but the biggest contribution will probably come from obtaining more lightcurves. Lightcurves can often provide pole directions when radar observations cannot, but obtaining lightcurves can be a major logistical challenge and they are often not available for many NEAs observed by radar.

Summary

The number of NEAs being observed annually with radar is approaching 100, but that is still only a fraction of the number that could be observed if telescope time, funding, personnel, equipment problems, and the ability to respond to targets-of-opportunity very rapidly were not issues.

Asteroid radar astronomy has made dramatic strides forward since publication of *Asteroids III*, the field is growing, and it has considerable scientific potential. New discoveries occur frequently, imaging resolutions are approaching the realm of planetary geology, and radar observations have become important in ways that were never imagined only a decade ago.

Acknowledgements

We thank D. J. Scheeres and an anonymous reviewer for comments that improved this manuscript. Part of this work was performed at the Jet Propulsion Laboratory, California Institute of Technology, under contract with the National Aeronautics and Space Administration (NASA). This material is based in part upon work supported by NASA under the Science Mission Directorate Research and Analysis Programs.

Table 1: NEAs With Radar-Detected Craters

Asteroid			H
1580	Betulia		14.5
4179	Toutatis		15.3
4183	Cuno		14.4
33342	1998	WT24	17.9
52760	1998	ML14	17.5
53319	1999	JM8	15.2
136849	1998	CS1	17.6
185851	2000	DP107	18.2
304330	2006	SX217	18.9
308635	2005	YU55	21.9
388188	2006	DP14	18.9
	2010	JL33	17.7

FIGURES

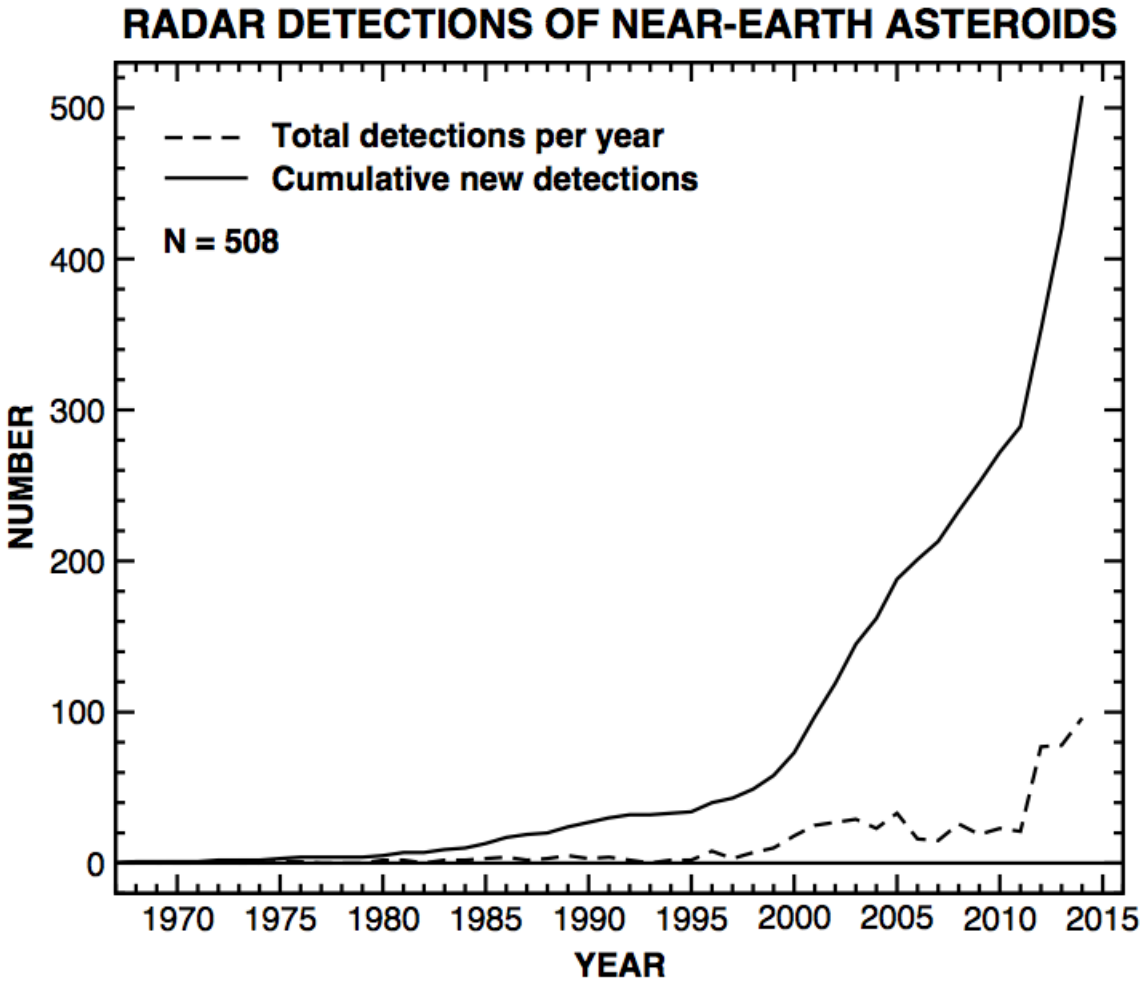

Figure 1
Number of near-Earth asteroid radar detections through the end of 2014. The increase in cumulative detections in 1999-2000 was caused in part by a surge of discoveries by LINEAR and by the order-of-magnitude increase in sensitivity at Arecibo after the upgrade. The increase in 2012 was the result of increased funding for Arecibo and greater access to telescope time at Arecibo and Goldstone.

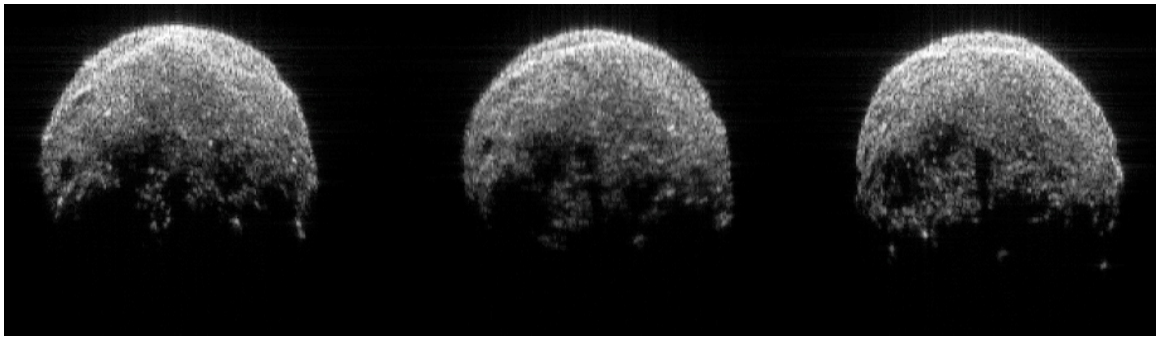

Figure 2
Bistatic Goldstone DSS-14/DSS-13 radar images of near-Earth asteroid 2005 YU55 obtained on 2011 November 9. Range increases down and Doppler frequency increases to the left, so rotation is clockwise. Range resolution is 3.75 m/row, but the data were double sampled, so each row corresponds to 1.875 m.

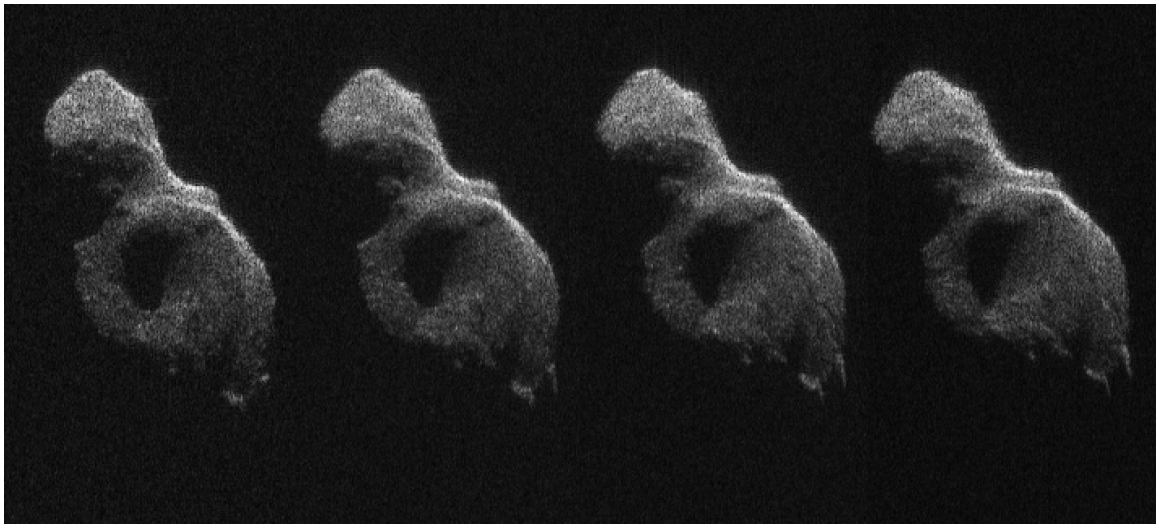

Figure 3
Bistatic Goldstone-Arecibo images of near-Earth asteroid 2014 HQ124 obtained on 2014 June 8. Each pixel has dimensions of 1.875 m x 0.00625 Hz.

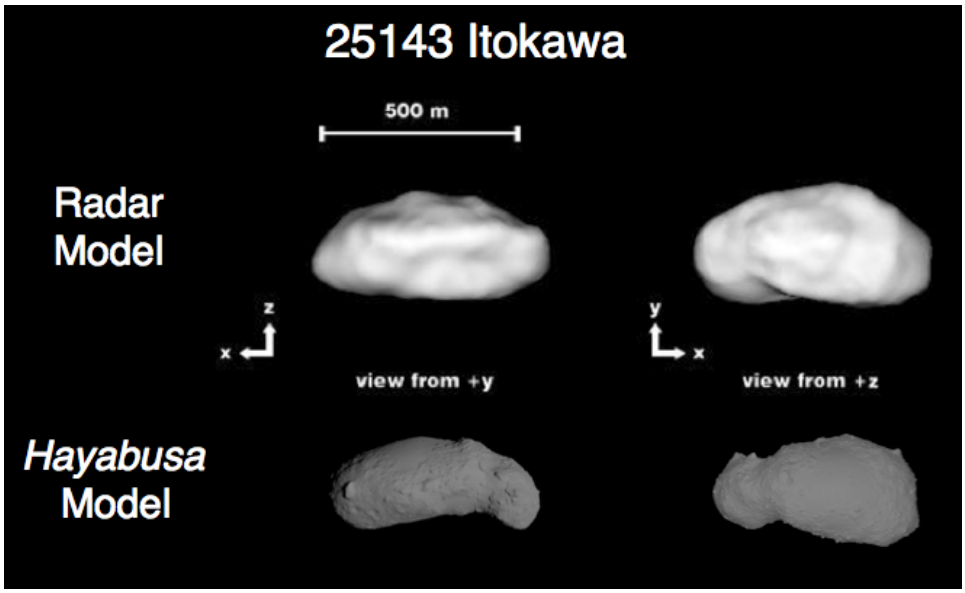

Figure 4
Two principal axis views of the Itokawa models estimated from inversion of radar images (top row, adapted from Ostro et al. 2005) and from *Hayabusa* spacecraft images (bottom row, adapted from Gaskell et al. 2008). The renderings are shown at the same orientations and approximately to scale. The lower hemisphere in the renderings on the left was not imaged by radar.

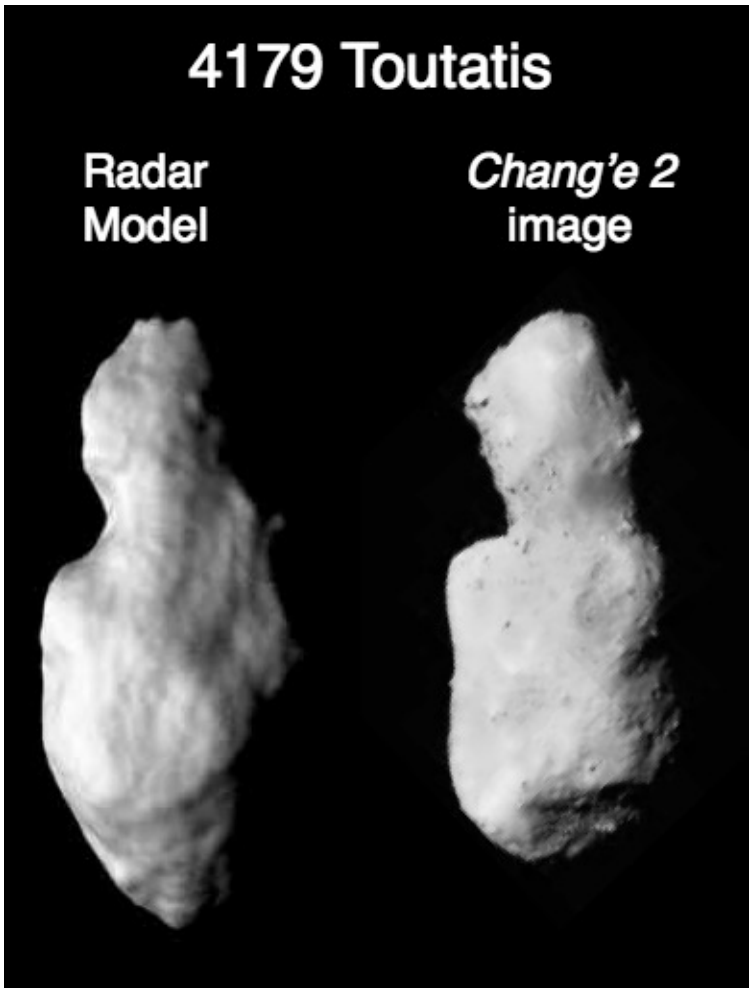

Figure 5
Comparison between the Hudson et al. (2003) radar-derived shape model of Toutatis and a representative image obtained by the *Chang'e 2* spacecraft (adapted from Huang et al. 2013). The orientations and scales are approximate and were estimated by eye. Illumination directions are similar.

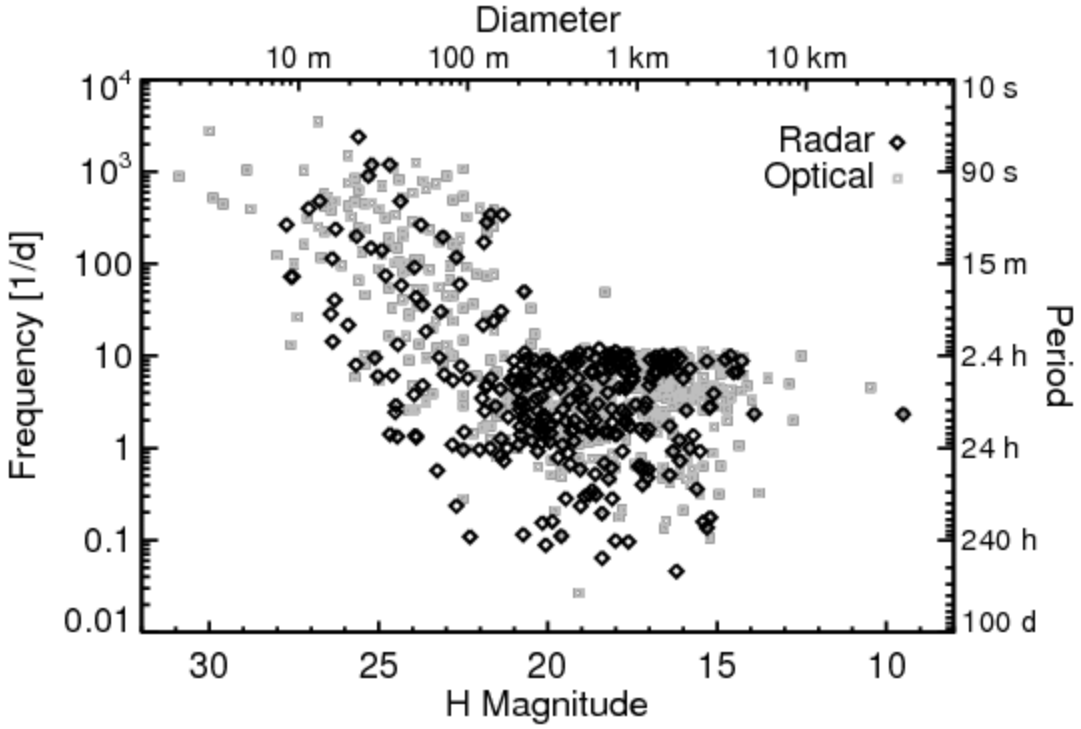

Figure 6
Spin-rate distribution of near-Earth asteroids as determined by optical and radar techniques (Taylor et al. 2012). Optical data (gray squares) are periods from the Warner lightcurve database (Warner et al., 2009; September 2014 update) with quality factors U >= 2; radar data (black diamonds) are estimated from echo bandwidths observed at Arecibo. There is broad agreement between the two techniques despite different observational biases, including the lack of slowly rotating small bodies. Diameters are computed from absolute magnitudes by assuming an optical albedo of 0.2.

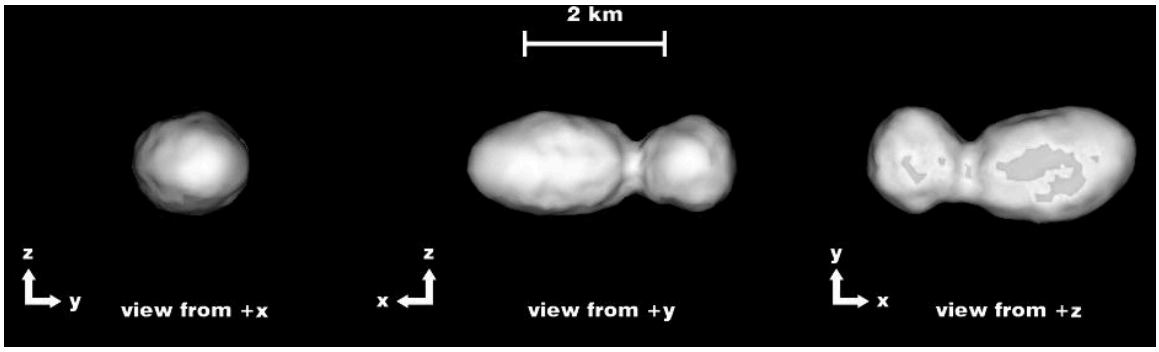

Figure 7
Principal axis views of the 1996 HW1 shape model (adapted from Magri et al. 2011). This is one of the most bifurcated NEAs modeled to date using delay-Doppler radar images.

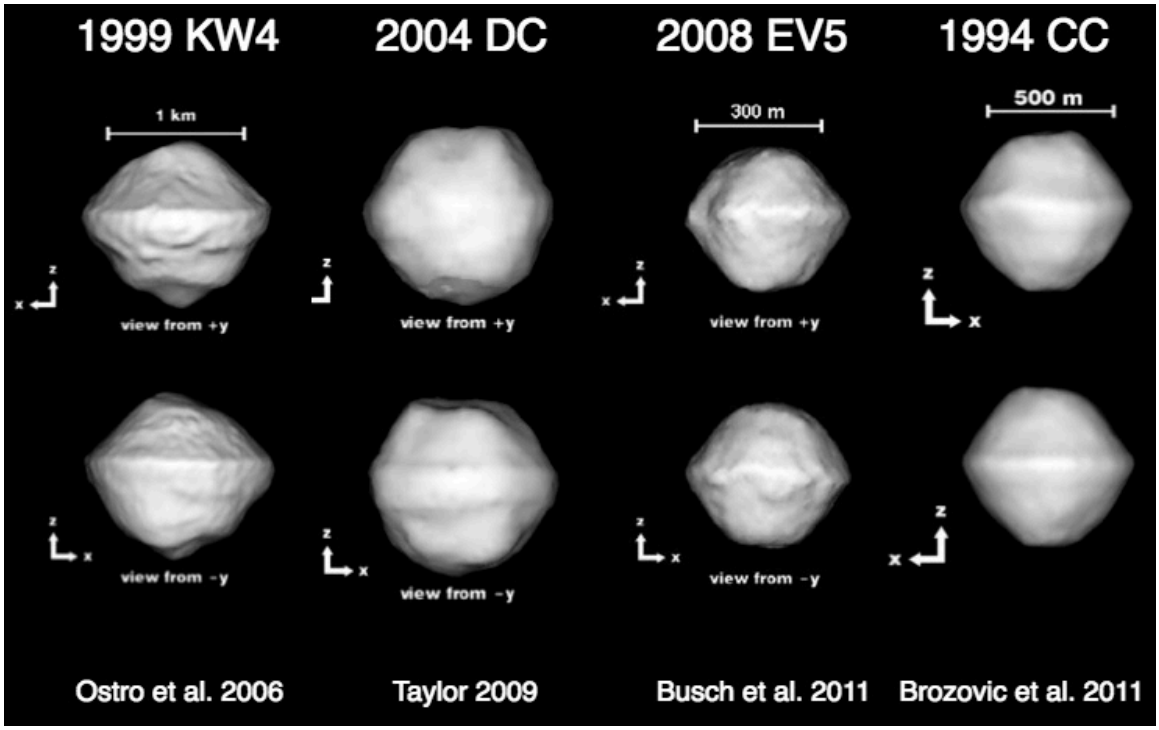

Figure 8
Model renderings of four near-Earth asteroids with evidence for oblate shapes. Each model is viewed along the + and - y-axes.

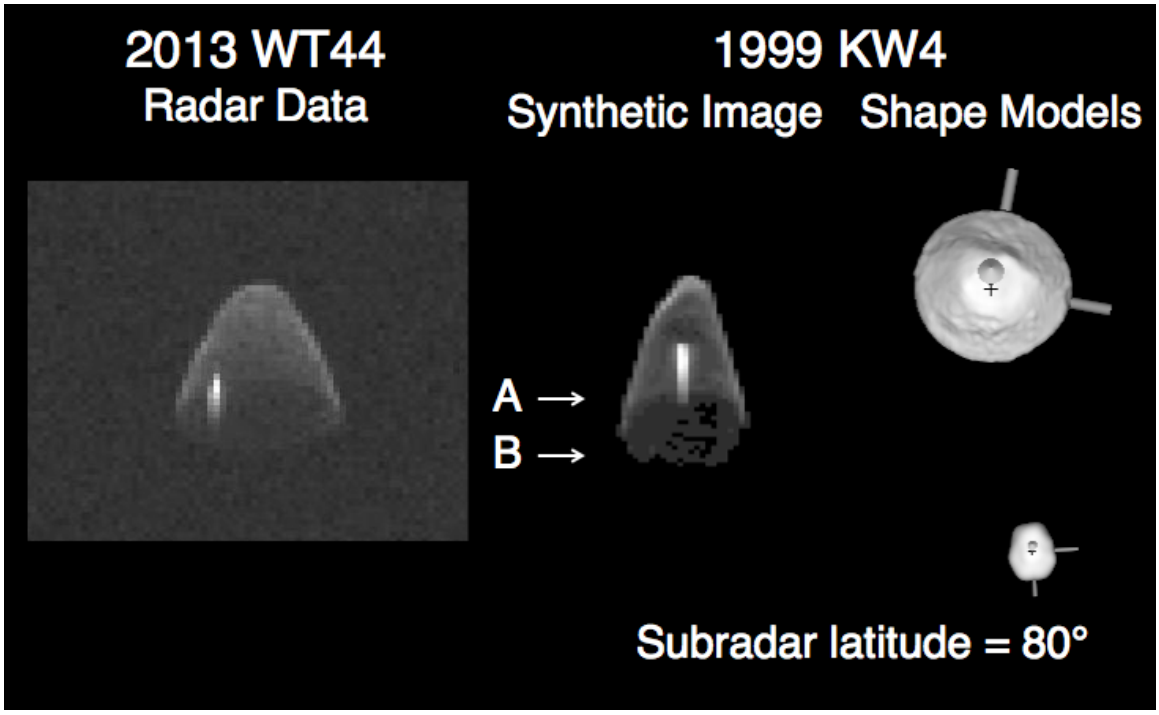

Figure 9
Comparison between observations of binary NEA 2013 WT44 and a synthetic radar image of binary 1999 KW4 viewed at a high subradar latitude. Left: Goldstone delay-Doppler image of 2013 WT44 obtained on 2014 March 20. Resolution = 18.75 m x 0.5 Hz. Right: Plane-of-sky renderings of the 1999 KW4 shape models viewed from a subradar latitude of 80 deg. Middle: Synthetic radar image of 1999 KW4 generated using the geometry of the models shown on the right. In the synthetic image, upper and lower arrows point to echoes from the near and far edges of the equatorial bulge.

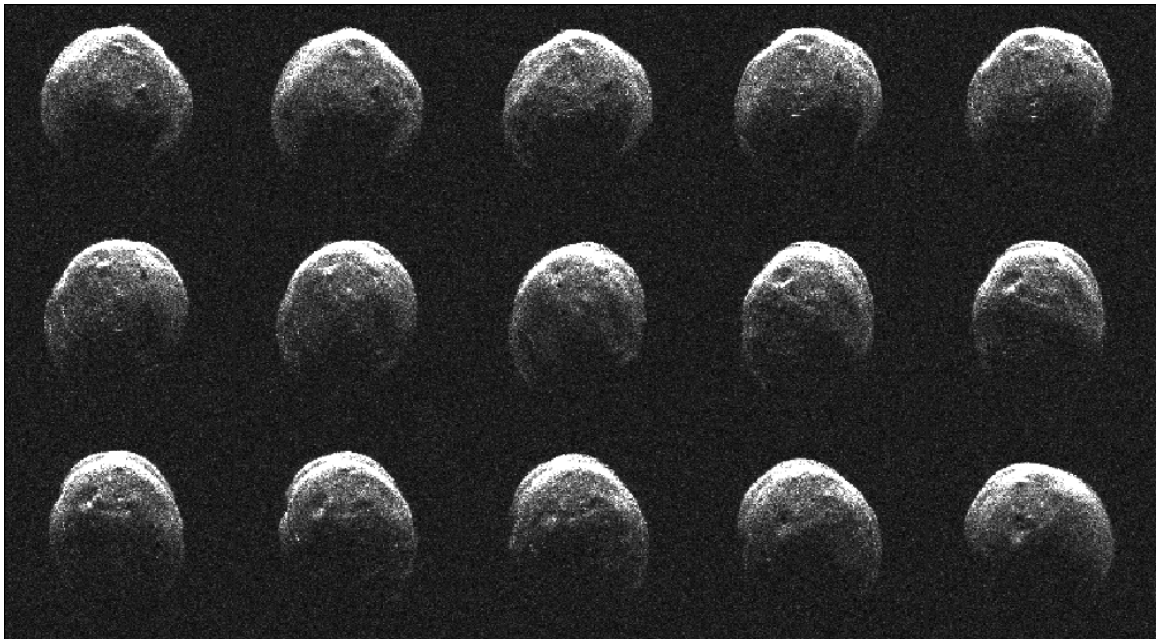

Figure 10
Arecibo images of 136849 1998 CS1 obtained on 2009 January 18. Resolution is 7.5 m x 0.09 Hz. Rotation is counterclockwise.

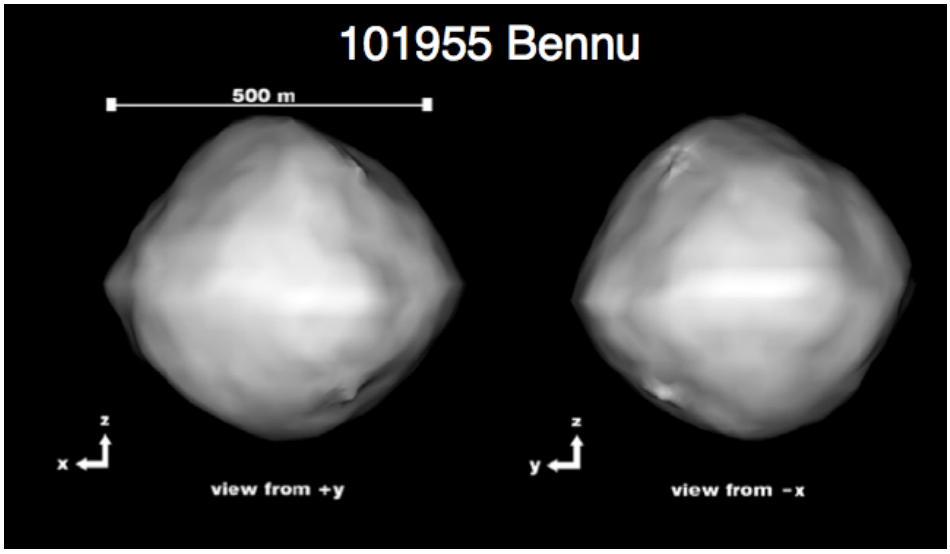

Figure 11
Renderings of the 3D model of 101955 Bennu (adapted from Nolan et al. 2013) viewed along the x- and y-axes.

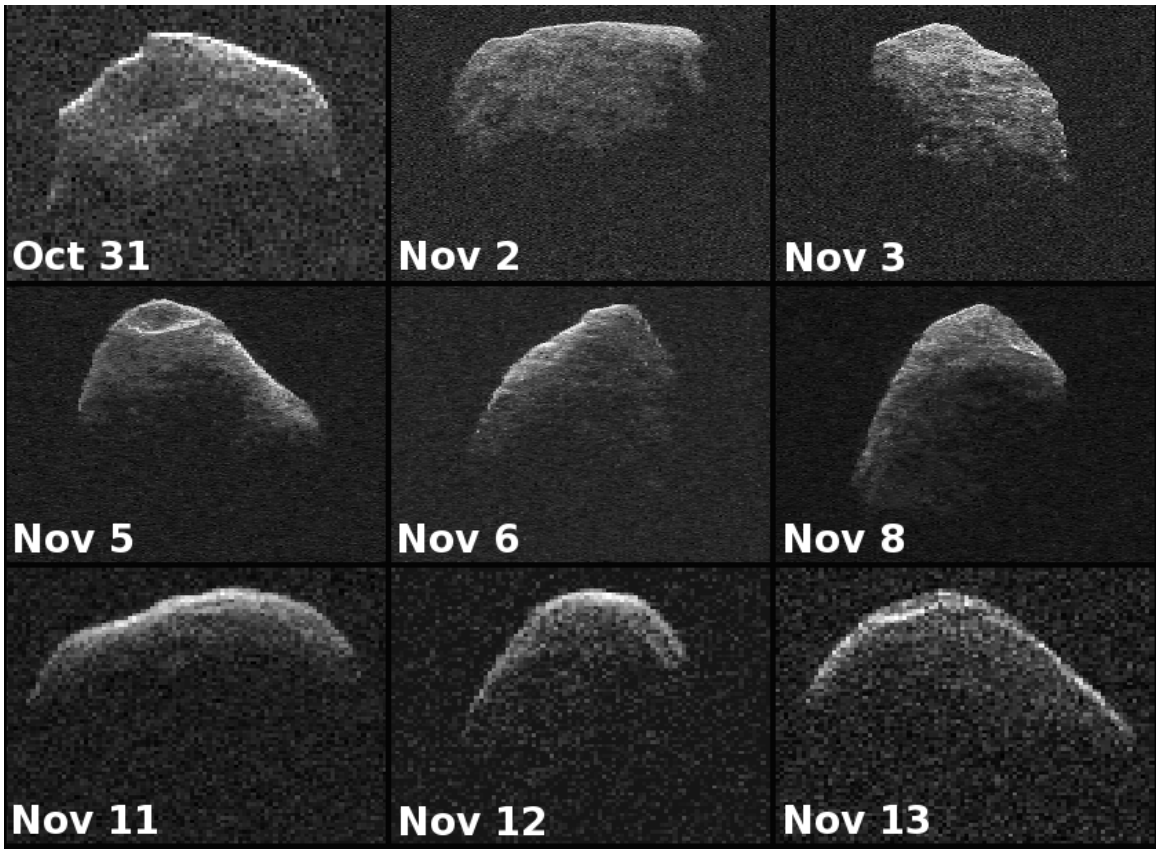

Figure 12

Images of 214869 2007 PA8 obtained at Goldstone during October-November 2012. Range resolutions are 18.75 m on Oct. 31 and Nov. 11-13; 7.5 m on Nov. 2, 3, and 8; and 3.75 m on Nov. 5 and 6. The highest resolutions were obtained on dates when the asteroid was closest to Earth and the signal-to-noise ratios were strongest. Each panel has the same delay-Doppler dimensions.

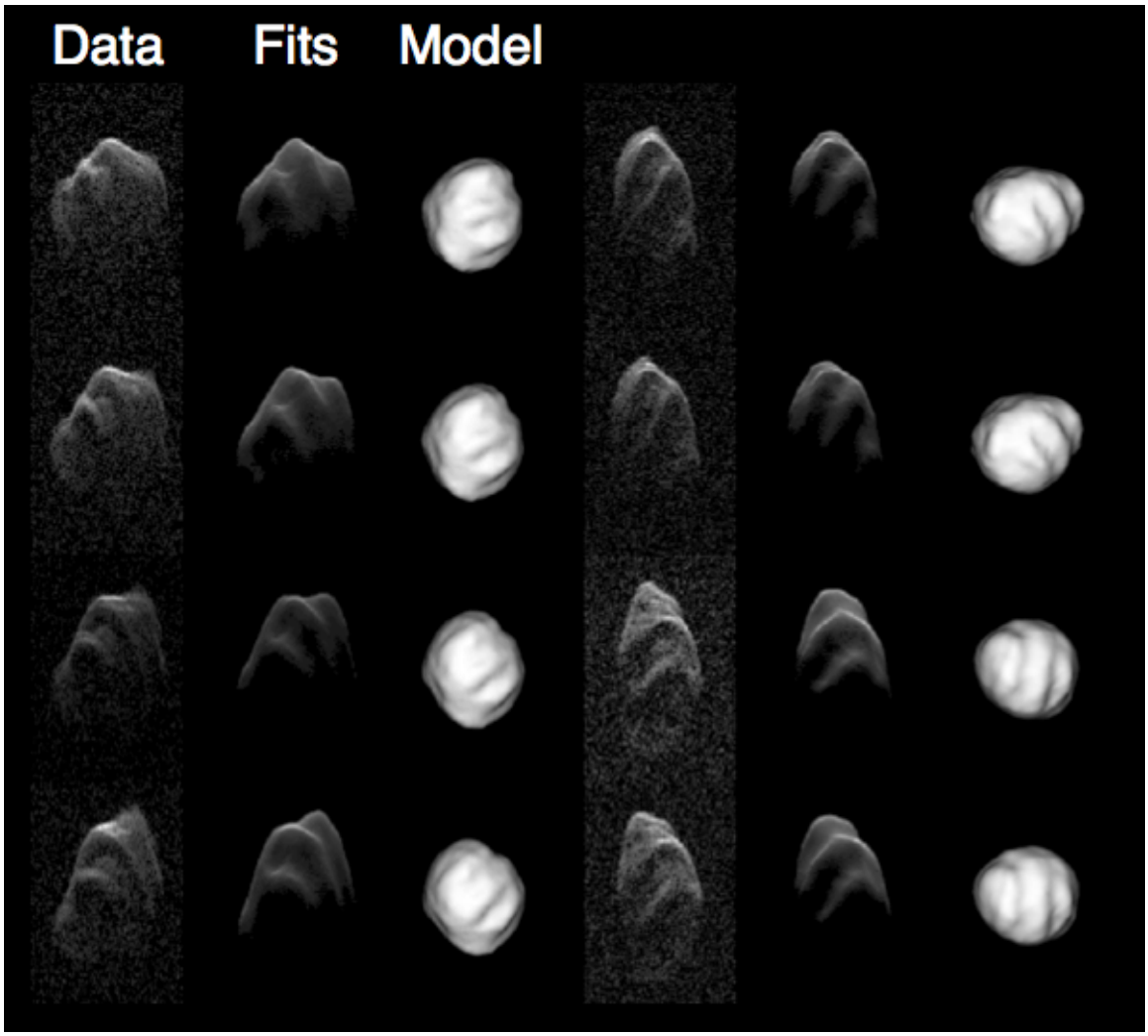

Figure 13
Selected Arecibo images, fits, and plane-of-sky views of the 2000 ET70 shape model (Naidu et al. 2013).

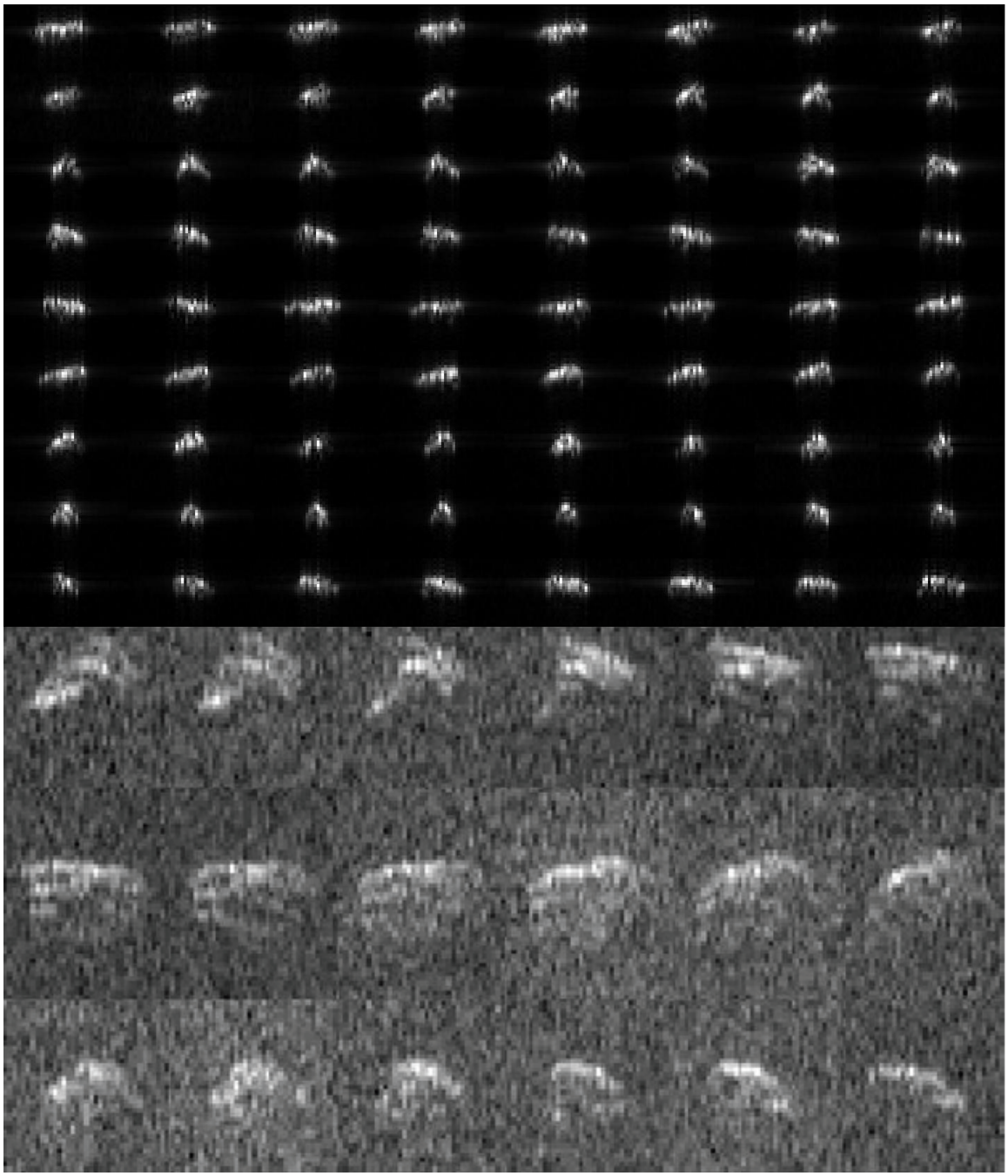

Figure 14
Goldstone images of two NEAs that are less than 100 m in diameter. Top: 367943 Duende (2012 DA14) imaged on 2013 Feb. 16. Duende has major axes of ~40 x 20 m, an angular shape, and is a non-principal axis rotator (Moskovitz et al. 2013). Bottom: 2013 ET images from 2013 Mar. 10. 2013 ET appears structurally complex, has a long axis of at least 40 m, and has alternating radar-dark and radar-bright regions. In each collage, the range resolution is 3.75 m, but the data were double sampled, so each row corresponds to 1.875 m.

References

Benner, L. A. M., and 12 colleagues (1999) Radar observations of asteroid 2063 Bacchus. *Icarus, 139*, 309-327.

Benner, L. A. M., and 10 colleagues (2002) Radar observations of asteroid 1999 JM8. *Meteorit. Planet. Sci., 37*, 779-792.

Benner, L. A. M., and 5 colleagues (2006) Near-Earth asteroid 2005 CR37: Radar images of a candidate contact binary. *Icarus, 182*, 474-481.

Benner, L. A. M., and 10 colleagues (2008) Near-Earth asteroid surface roughness depends on compositional class. *Icarus, 198*, 294-304.

Benner, L. A. M., and 13 colleagues (2009) Arecibo and Goldstone radar images of near-Earth asteroid (136849) 1998 CS1. *Bull. Am. Astron. Soc., 41*, 1083. [abstract]

Benner, L., and 11 colleagues (2014) *Asteroids, Comets, Meteors 2014*. Arecibo and Goldstone radar evidence for boulders on near-Earth asteroids. [abstract]

Benner, L. A. M., and 16 colleagues (2014) Goldstone and Arecibo radar images of near-Earth asteroid 2014 HQ124. *Bull. Am. Astron. Soc., 46,* 49.01. [abstract]

Bottke, W. F., and 3 colleagues (2002) The effect of Yarkovsky thermal forces on the dynamical evolution of asteroids and meteoroids. In Asteroids III, W. F. Bottke, A. Cellino, P. Paoliccchi, and R. P. Binzel. Eds. Tucson: Univ. of Arizona Press, pp. 395-408.

Bottke, W.F.,and 3 colleagues (2006) The Yarkovsky and YORP effects: Implications for asteroid dynamics. *Ann. Rev. Earth Planet. Sci.*, *34*, 157-191.

Brozovic, M., and 10 colleagues (2009) Radar observations and a physical model of asteroid 4660 Nereus, a prime space mission target. *Icarus, 201*, 153-166.

Brozovic, M., and 9 colleagues (2010) Radar observations and a physical model of contact binary asteroid 4486 Mithra. *Icarus, 208*, 207-220.

Brozovic, M., and 21 colleagues (2011) Radar observations and physical modeling of triple near-Earth asteroid (136617) 1994 CC. *Icarus, 216*, 241-256.

Brozovic, M., and 3 colleagues (2013) Goldstone radar imaging of near-Earth asteroid (214869) 2007 PA8. *EPSC Abstracts, 8*, 2013-296.

Busch, M. W., and 9 colleagues (2006) Radar and Optical Observations and Physical Modeling of Near-Earth asteroid 10115 (1992 SK). *Icarus, 181*, 145-155.

Busch, M. W., and 14 colleagues (2007) Physical modeling of near-Earth asteroid (29075) 1950 DA. *Icarus, 190*, 608-621.

Busch, M. W., and 9 colleagues (2008) Physical properties of near-Earth asteroid (33342) 1998 WT24. *Icarus, 195*, 614-621.

Busch, M. W., and 6 colleagues (2010) Determining asteroid spin states using radar speckles. *Icarus, 209*, 535-541.

Busch, M. W., and 12 colleagues (2011) Radar observations and the shape of near-Earth asteroid 2008 EV5. *Icarus, 212*, 649-660.

Busch, M.W., and 6 colleagues (2011) Twenty years of Toutatis. *EPSC-DPS Joint meeting 2011*, 297 [abstract].

Busch, M. W., and 16 colleagues (2012) Shape and spin of near-Earth asteroid 308635 (2005 YU55) from radar images and speckle tracking. *Asteroids, Comets, Meteors 2012*, 39. [abstract]

Capek, D., and Vokrouhlicky, D. (2004). The YORP effect with finite thermal conductivity. *Icarus*, *172*, 526-536.

Chesley, S. R., and 9 colleagues (2003) Direct detection of the Yarkovsky effect via radar ranging to asteroid 6489 Golevka. *Science, 302*, 1739-1742.

Chesley, S. R., and 7 colleagues (2008) Direct estimation of Yarkovsky accelerations on Near-Earth Asteroids. A*steroids, Comets, Meteors 2008*, 8330. [abstract]

Chesley, S. R., and 15 colleagues (2014). Orbit and bulk density of the OSIRIS-REx target Asteroid (101955) Bennu. *Icarus, 235*, 5-22.

Davarian, F. (2011) Uplink arraying for solar system radar and radio science. Proc. *IEEE*, *99*, 783-793.

Descamps, P., and 18 colleagues (2011). Triplicity and physical characteristics of asteroid (216) Kleopatra. *Icarus, 211*, 1022-1033.

Di Martino, M., and 13 colleagues (2004) Results of the first Italian planetary radar experiment. *Planet. Space Sci., 52*, 325-330.

Durech, J., and 11 colleagues (2008) Detection of the YORP effect in the asteroid (1620) Geographos. *Astron. Astrophys., 489*, L25-L28.

Fang, J., and 5 colleagues (2011) Orbits of near-Earth asteroid triples 2001 SN263 and 1994 CC: Properties, origin, and evolution. *Astron. J., 141*, 154.

Farnocchia, D., and 5 colleages (2013a) Near Earth Asteroids with measureable Yarkovsky effect. *Icarus, 224*, 1-13.

Farnocchia, D., and 7 colleagues (2013b) Yarkovsky-driven impact risk analysis for asteroid (99942) Apophis. I*carus, 224*, 192-200.

Farnocchia, D., and Chesley, S. R. (2014) Assessment of the 2880 impact threat from asteroid (29075) 1950 DA. *Icarus*, *229*, 321-327.

Gaskell, R., and 8 colleagues (2008) Gaskell Itokawa shape model V 1.0. HAY-A-AMICA-5-ITOKAWASHAPE-V1.0. NASA Planetary Data System.

Giorgini, J. D., and 13 colleagues (2002) Asteroid 1950 DA's encounter with Earth: Physical limits of collision probability prediction. *Science, 296*, 132-136.

Giorgini, J. D., and 4 colleagues (2008) Predicting the Earth encounters of (99942) Apophis. *Icarus, 193*, 1-19.

Harmon, J. K., and 3 colleagues (2010) Radar observations of 8P/Tuttle: A contact-binary comet. *Icarus, 207*, 499-502.

Harmon, J. K., and 4 colleagues (2011) Radar observations of comet 103P/Hartley 2. *Ap. J. Lett., 734*, L2.

Hirabayashi, M., and Scheeres, D. Stress and failure analysis of rapidly rotating asteroid (29075) 1950 DA, *Ap. J. Lett.*, in press.

Huang, J., and 27 colleagues (2013) The ginger-shaped asteroid 4179 Toutatis: New observations from a successful flyby of Chang'e-2. *Nature Scientific Reports, 3*: 3411.

Hudson, S. (1993) Three-dimensional reconstruction of asteroids from radar observations. *Remote Sens. Rev., 8*, 195-203.

Hudson, R. S., and Ostro, S. J. (1994) Shape of asteroid 4769 Castalia (1989 PB) from inversion of radar images. *Science, 263*, 940-943.

Hudson, R. S., and Ostro, S.J. (1995) Shape and non-principal axis spin state of asteroid 4179 Toutatis. *Science, 270*, 84-86.

Hudson, R. S., and 26 colleagues (2000) Radar observations and physical model of asteroid 6489 Golevka. *Icarus, 148*, 37-51.

Hudson, R. S., Ostro, S.J., and Scheeres, D.J. (2003) High-resolution model of asteroid 4179 Toutatis. *Icarus, 161*, 346-355.

Kaasalainen, M., and 21 colleagues (2004) Photometry and models of eight near-Earth asteroids. *Icarus, 167*, 178-196.

Kaasalainen, M., and 4 colleagues (2007) Acceleration of the rotation of asteroid 1862 Apollo by radiation torques. *Nature*, *446*, 420-422.

Lowry, S.C., and 10 colleagues (2007) Direct detection of the asteroidal YORP effect. *Science*, *316*, 272-274.

Lowry, S.C., and 11 colleagues (2014) The internal structure of asteroid (25143) Itokawa as revealed by detection of YORP spin-up. *Astron. Astrophys., 562*, A48.

Magri, C., and 3 colleagues (2007) A radar survey of main-belt asteroids: Arecibo observations of 55 objects during 1999-2003. *Icarus, 186*, 126-151.

Magri, C., and 6 colleagues (2007) Radar observations and a physical model of asteroid 1580 Betulia. *Icarus, 186*, 152-177.

Magri, C., and 25 colleagues (2011) Radar and photometric observations and shape modeling of contact binary near-Earth asteroid (8567) 1996 HW1. *Icarus, 214*, 210-227.

Margot, J. L., and 7 colleagues (2002) Binary asteroids in the near-Earth object population. *Science, 296*, 1445-1448.

Margot, J. L., and 4 colleagues (2007) Large longitude libration of Mercury reveals a molten core. *Science, 316*, 710-714.

Margot, J.L., and 9 colleagues (2012) Mercury's moment of inertia from spin and gravity data. *J. Geophys. Res., 117*, E00L09.

Milani, A., and 5 colleagues (2009) Long term impact risk for (101944) 1999 RQ36. *Icarus, 203*, 460-471.

Moskovitz, N., and 19 colleagues (2013) The near-Earth asteroid 2012 DA14. *Bull. Am. Astron. Soc., 45*, abstract 101.03.

Naidu, S. P., and 9 colleagues (2013) Radar imaging and physical characterization of near-Earth asteroid (162421) 2000 ET70. *Icarus, 226*, 323-335.

Naidu, S. P., and Margot, J.L. (2015) Near-Earth asteroid satellite spins under spin-orbit coupling. *Astron. J.,* 149, 80.

Naidu, S. P., and 9 colleagues (2015) Radar imaging and characterization of binary near-Earth asteroid (185851) 2000 DP107. *Astron. J.,* submitted.

Nechaeva, M., and 19 colleagues (2013). First results of the VLBI experiment on radar location of the asteroid 2012 DA14. *Baltic Astron., 22*, 341-346.

Nolan, M.C., and 10 colleagues (2013) Shape model and surface properties of the OSIRIS-REx target asteroid (101955) 1999 RQ36 from radar and lightcurve observations. *Icarus, 226*, 629-640.

Shapiro, I.I., Ash, M.E., and Smith, W.B. (1968) Icarus-further confirmation of relativistic perihelion precession. *Phys. Rev. Lett., 20*, 1517-1518.

Nugent, C.R., and 3 colleagues (2012) Detection of semi-major axis drifts in 54 Near-Earth Asteroids: New measurements of the Yarkovsky effect. *Astron. J., 144*, 60-72.

Ostro, S. J. (1993) Planetary radar astronomy. *Rev. Mod. Phys., 65*, 1235-1279.

Ostro, S. J., and 15 colleagues (1999) Asteroid 4179 Toutatis: 1996 radar observations. *Icarus, 137*, 122-139.

Ostro, S. J., and 8 colleagues (2000) Radar Observations of Asteroid 216 Kleopatra. *Science, 288*, 836-839.

Ostro, S. J., and 6 colleagues (2002) Asteroid radar astronomy. In *Asteroids III* (W. Bottke, A. Cellino, P. Paolicchi, and R. P. Binzel, eds.), Univ. of Arizona Press, Tucson, pp. 151-168.

Ostro, S. J., and Giorgini, J. D. (2004). The role of radar in predicting and preventing asteroid and comet collisions with Earth. In *Mitigation of Hazardous Comets and Asteroids* (M. J. S. Belton, T. H. Morgan, N. Samarasinha, and D. K. Yeomans, eds.), Cambridge Univ. Press, Cambridge, pp. 38-65.

Ostro, S. J., and 15 colleagues (2004) Radar observations of asteroid 25143 Itokawa (1998 SF36). *Meteorit. Planet. Sci., 39*, 407-424.

Ostro, S. J., and 12 colleagues (2005) Radar observations of Itokawa in 2004 and improved shape estimation. *Meteorit. Planet. Sci., 40*, 1563-1574.

Ostro, S. J., and 15 colleagues (2006) Radar imaging of binary near-Earth asteroid (66391) 1999 KW4. *Science, 314*, 1276-1280.

Ostro, S. J., and 7 colleagues (2010) Radar imaging of asteroid 7 Iris. *Icarus, 207*, 285-294.

Pravec, P., and 58 colleagues. (2006) Photometric survey of binary near-Earth asteroids. *Icarus*, *181*, 63-93.

Rivkin, A.S., and 4 colleagues (2000) The nature of M-class asteroids from 3 μm observations. *Icarus, 145*, 351-368.

Rozitis, B., and 3 colleagues (2013) A thermophysical analysis of the (1862) Apollo Yarkovsky and YORP effects. *Astron. Astrophys., 555*, A20.

Rozitis, B., MacLennan, E., and Emery, J.P. (2014) Cohesive forces prevent the rotational breakup of rubble-pile asteroid (29075) 1950 DA. *Nature*, *512*, 174-176.

Rubincam, D.P. (2000) Radiative spin-up and spin-down of small asteroids. *Icarus*, *148*, 2-11.

Saba, L., and 15 colleagues (2005) The Sardinia Radio Telescope as a radar for the study of near-Earth objects and space debris. *Mem. S. It. Suppl*, *6*, 104-109.

Saito, J., and 33 colleagues (2006) Detailed images of asteroid 25143 Itokawa from Hayabusa. *Science, 312*, 1341-1344.

Scheeres, D. J., and 5 colleagues (2005). Abrupt alteration of asteroid 2004 MN4's spin state during its 2029 Earth flyby. *Icarus, 178*, 281-283.

Shepard, M. K., and 12 colleagues (2006) Radar, optical, and thermal observations of the binary near-Earth asteroid 2002 CE26. *Icarus, 184*, 198-210.

Shepard, M. K., and 14 colleagues (2008a) Multi-wavelength observations of asteroid 2100 Ra-Shalom. *Icarus, 193*, 20-38.

Shepard, M. K., and 18 colleagues (2008b) A radar survey of X- and M-class asteroids. *Icarus, 195*, 184-205.

Shepard, M. K., and 9 colleagues (2008c) Radar observations E-class asteroids 44 Nysa and 434 Hungaria. *Icarus, 195*, 220-225.

Shepard, M. K., and 12 colleagues (2010) A radar survey of M- and X-class asteroids. II. Summary and synthesis. *Icarus, 208*, 221-237.

Shepard, M. K., and 9 colleagues (2011) Radar observations of asteroids 64 Angelina and 69 Hesperia. *Icarus, 215*, 547-551.

Shepard, M. K., and 15 colleagues (2015) A radar survey of M- and X-class asteroids. III. Insights into their compositions, hydration state, and structure. *Icarus*, *245*, 38-55.

Sierks, H., and 57 colleages (2011) Images of asteroid 21 Lutetia: A remnant planetesimal from the early solar system. *Science, 334*, 487-490.

Slade, M.A., and 6 colleagues (2010) First results of the new Goldstone delay-Doppler radar chirp imaging system. *Bull. Am. Astron. Soc., 42*, 1080 [abstract]

Slade, M. A., Benner, L.A.M., and Silva, A. (2011) Goldstone Solar System Radar Observatory: Earth-based planetary mission support and unique science results. *Proceedings IEEE, 99*, 757-769.

Springmann, A., and 3 colleagues 2013. Are the radar scattering properties of near-Earth asteroids correlated with size, shape, or spin? *Lunar Planet. Sci. Conf., 44*, 2915 [abstract]

Takahashi, Y., Busch, M.W., and Scheeres, D.J. (2013) Spin state and moment of inertia characterization of 4179 Toutatis. *Astron. J., 146*, 95.

Taylor, P. A., and 11 colleagues (2007) Increasing spin rate of asteroid 54509 (2000 PH5) a result of the YORP effect. *Science, 316*, 274-277.

Taylor, P. A. (2009). Tidal interactions in binary asteroid systems. Ph.D. Thesis, Cornell University.

Taylor, P.A., and 3 colleagues (2012) The shape and spin Distributions of near-Earth asteroids observed with the Arecibo radar system. *Bull. Am. Astron. Soc.*, *44*, Abstract 302.07.

Virkki, A., Muinonen, K., Penttila, A. (2014) Inferring asteroid surface properties from radar albedos and circular polarization ratios. *Meteorit. Planet. Sci.*, *59*, 86-94.

Vokrouhlicky, D., Milani, A., and Chesley, S.R. (2000) Yarkovsky effect on small near-Earth asteroids: Formulation and examples. *Icarus, 148*, 118-138.

Vokrouhlicky, D., and 3 colleagues (2005a) Yarkovsky effect opportunities. I. Solitary asteroids. *Icaru,s 173*, 166-184.

Vokrouhlicky, D., and 3 colleagues (2005b) Yarkovsky effect opportunities. II. Binary systems. *Icarus, 179*, 128-138.

Volquardsen, E.L., Rivkin, A.S., and Bus, S. J. (2007) Composition of hydrated near-Earth object (100085) 1992 UY4. *Icarus*, *187*, 464-468.

Zou, X., and 5 colleagues (2014) The preliminary analysis of the 4179 Toutatis snapshots of the Chang'E-2 flyby. *Icarus, 229*, 348-354.